#### **RESEARCH ARTICLE**



## Evidence for primitive magma storage and eruption following prolonged equilibration in thickened crust

Heather Winslow 1 • Philipp Ruprecht 1 • Mark Stelten 2 • Alvaro Amigo 3,4

Received: 24 January 2020 / Accepted: 15 September 2020 © International Association of Volcanology & Chemistry of the Earth's Interior 2020

#### **Abstract**

In continental arcs, the exposure of primitive eruptive products at the surface is typically a result of rapid magmatic transfer through the crust. As a result, the initially primitive magma experiences minimal crustal residence and thus insignificant differentiation towards more evolved products. This rapid transfer of primitive magma through thickened crust is commonly recorded from smaller, monogenetic cinder cones. Manantial Pelado (35.5° S) is a long-lived stratocone in the Southern Andean Volcanic Zone (SVZ) overlying thick continental crust (45–50 km) that produces almost exclusively mafic material. As Manantial Pelado is surrounded by extensive silicic volcanism, the study of its mafic exposure as a stratocone can be used to further understand magmatic origins of long-lived volcanic systems. Our study uses textural, geochemical, and geochronological data from lavas collected from Manantial Pelado to characterize its magmatic petrogenesis, assess the primitive nature, and explain processes in the crust within the SVZ. A geologic description of the volcano reveals a mostly monotonous eruptive history of basaltic andesites that are now accessible through glacially carved valleys. New 40Ar/39Ar dating constrains most of the volcano's cone constructing phase to last from ~220 to 190 ka. At ~30 ka, small-volume activity and different petrography of more intermediate magmas were present reflecting a change in the volcano's character. A combination of the whole-rock and mineral-scale data reveals that basaltic andesites at Manantial Pelado are among the most primitive magmas in the thickened crust of the SVZ. Evidence for this primitive signature consists of textural and zonation patterns in olivine, the presence of Cr-spinel in olivine cores, and elevated Fo and Ni content within olivine cores. This data combined with elemental diffusion modeling provides evidence for a primitive signature for these lavas. Intermediate Fo olivines with uniform core compositions (Fo<sub>80–84</sub>) suggest that basaltic andesites reside in the crust in quasi-closed system environments for extended storage prior to eruption (~ 25-6000 years). Diffusive equilibration in those intermediate Fo olivines masks the primitive nature of the magmas. These results suggest that mafic magmas can have a protracted storage history in the crust that does not significantly alter their primitive bulk composition before reaching the surface. We argue that these are important processes in understanding the magmatic origin of long-lived systems and the presence of compositionally homogenous olivines at intermediate Fo content may represent cryptic evidence for recharge with primitive magmas that experienced prolonged crustal storage.

Keywords Southern Andes · Mafic mush storage · Diffusive equilibration · Flat olivine cores · Manantial Pelado

Editorial responsibility: N. Métrich

**Electronic supplementary material** The online version of this article (https://doi.org/10.1007/s00445-020-01406-3) contains supplementary material, which is available to authorized users.

Heather Winslow hwinslow@nevada.unr.edu

Published online: 09 October 2020

- University of Nevada, Reno, 1664 N Virginia St, Reno, NV 89557, USA
- United States Geological Survey Menlo Park, 345 Middlefield Rd, Menlo Park, CA 94025, USA
- Servicio Nacional de Geología y Minería (SERNAGEOMIN). Red Nacional de Vigilancia Volcánica, Santiago, Chile
- Andean Geothermal Center of Excellence (CEGA, Fondap-CONICYT 15090013), Santiago, Chile

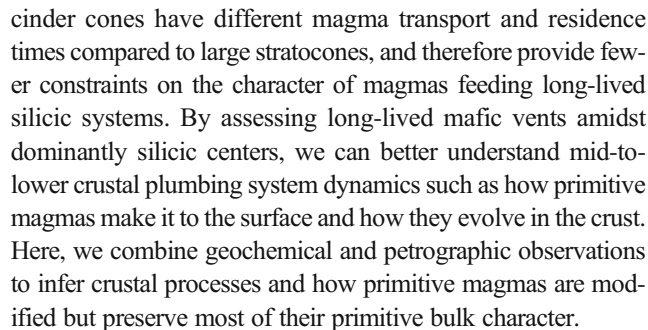


69 Page 2 of 24 Bull Volcanol (2020) 82:69

#### Introduction

Mafic magmas contribute heat, mass, and volatile elements to the crust and feed evolved magma systems. These contributions sustain the presence of long-lived shallow magma reservoirs (Grunder 1987; Dungan et al. 2001; Bachmann and Bergantz 2003; Wehrmann et al. 2014a). Mafic input controls and modulates magma composition, alters the eruptibility and eruptive behavior of stored magmas, and affects the frequency of eruption (Ruprecht and Bachmann 2010; Turner et al. 2016). Constraining mafic input is difficult in areas of thickened crust, such as the Andes, because the mostly elusive lower crust removes mantle parentage through deep-seated magma mixing, assimilation, storage, and homogenization (MASH; Hildreth and Moorbath 1988; Dufek and Bergantz 2005; Annen et al. 2006). The fact that mafic magmas are able to erupt though regions of thickened crust highlights that mafic pathways can exist within regions of otherwise extensive silicic volcanism (Hildreth et al. 2010; Salas et al. 2017; Burns et al. 2019).

While mafic centers play a major role in understanding regional magma genesis, the dearth of such centers in parts of the Southern Andes where the crust is thickened limit our ability to refine our models for lower crustal processes and parental compositions for nearby evolved systems. Exposed crustal sections of lower-to-middle crust may reveal some of these processes (Walker et al. 2015); however, plutons are continuously overprinted by numerous magmatic events and thus are limited to the cumulative impact of magmatism. Instead, volcanic deposits tap an individual magmatic system at depth and provide isolated snapshots in time. This can be used to distill specific magmatic processes and constraints. The most extensive work on the primitive magmatism in this region of the Andes was conducted at the Tatara-San Pedro Volcanic Complex (TSPC), where a detailed reconstruction of the eruptive history revealed a range of mafic parental magmas (Dungan et al. 2001). A regional study using whole-rock geochemistry also found only a few centers that erupt primitive magmas in this region (Hildreth et al. 2010). In addition, some constraints have been deduced from mafic enclaves in otherwise silicic eruptions within the Southern Andes (Ruprecht et al. 2012). More recently, two tephra studies focused on olivine-bearing small cinder cones between 34.5° S and 38.0° S (Jacques et al. 2013) and 33° S and 43° S (Wehrmann et al. 2014b), respectively, to document the geochemical variations across and along the Southern Andean Volcanic Zone (SVZ; 33° S-46° S). The latter study used melt inclusions and whole-rock geochemistry and found that mafic melts can ascend through thick continental crust without being influenced by crustal assimilation. While the cinder cone studies targeted mafic compositions, most of their compositions did not exceed 5.5-6 wt% MgO which is not considered primitive. Additionally, the focus was primarily on what the geochemistry can elucidate, drawing little evidence from petrographic observations. Moreover, the small-volume



One location in the SVZ where mafic contribution is dominant is at the Pleistocene stratocone Manantial Pelado (35.5° S. 70.8° W; Fig. 1). Manantial Pelado is a rare location in this part of the Andes producing near-primitive arc magmas while it sits atop thickened crust (Hildreth and Drake 1992). Centers surrounding Manantial Pelado are predominantly intermediate-tosilicic such as the Descabezado Grande-Cerro Azul Volcanic Complex and Laguna del Maule (Fig. 1b; Hildreth et al. 1984; Hildreth and Drake 1992; Ruprecht et al. 2012; Andersen et al. 2017). Manantial Pelado is an ideal field site to assess the role and contribution of mafic magmas because its glacially carved valleys expose a long eruptive history revealing its dominantly mafic activity (Hildreth and Drake 1992). Thus, we can use Manantial Pelado to elucidate the area's primitive history, determine a mafic baseline, and address how long-lived mafic systems operate and are fundamentally different to mafic magmas erupted at monogenetic cinder cones. In particular, we find that mineralscale and textural evidence point towards quasi-closed system processes combined with evolution in small mush regions that hide the near-primitive nature of Manantial Pelado magmas.

The paper is divided into two parts. First, we briefly describe Manantial Pelado, its eruptive style and history, and we present age constraints for its activity. We then focus on the petrographic and geochemical diversity and discuss in particular the magmatic processes that modify the most mafic magmas in this long-lived stratocone.

#### **Geologic setting**

Manantial Pelado sits within the transitional segment of the SVZ in the Chilean Andes, which is an exemplary continental arc known for its systematic changes in crustal thickness (Fig. 1; Hildreth and Moorbath 1988). Thick crust ( $\sim$  60 km) in the northern SVZ is the result of compression from ENE-trending ( $\sim$ 080° azimuth) oblique subduction of the Nazca plate beneath the South American plate at a rate of  $\sim$ 7–9 cm/year (Stern 2004). Crustal shortening leads to thickening of the overriding plate (Ramos et al. 1996; Tassara and Echaurren 2012). Southward, the crust of the SVZ thins to  $\sim$ 30 km (Hildreth and Moorbath 1988; Stern 2004). On the basis of a 3D density model between 20° S–45° S that resolved the mantle-crust structure and showed in detail the southward



Bull Volcanol (2020) 82:69 Page 3 of 24 69

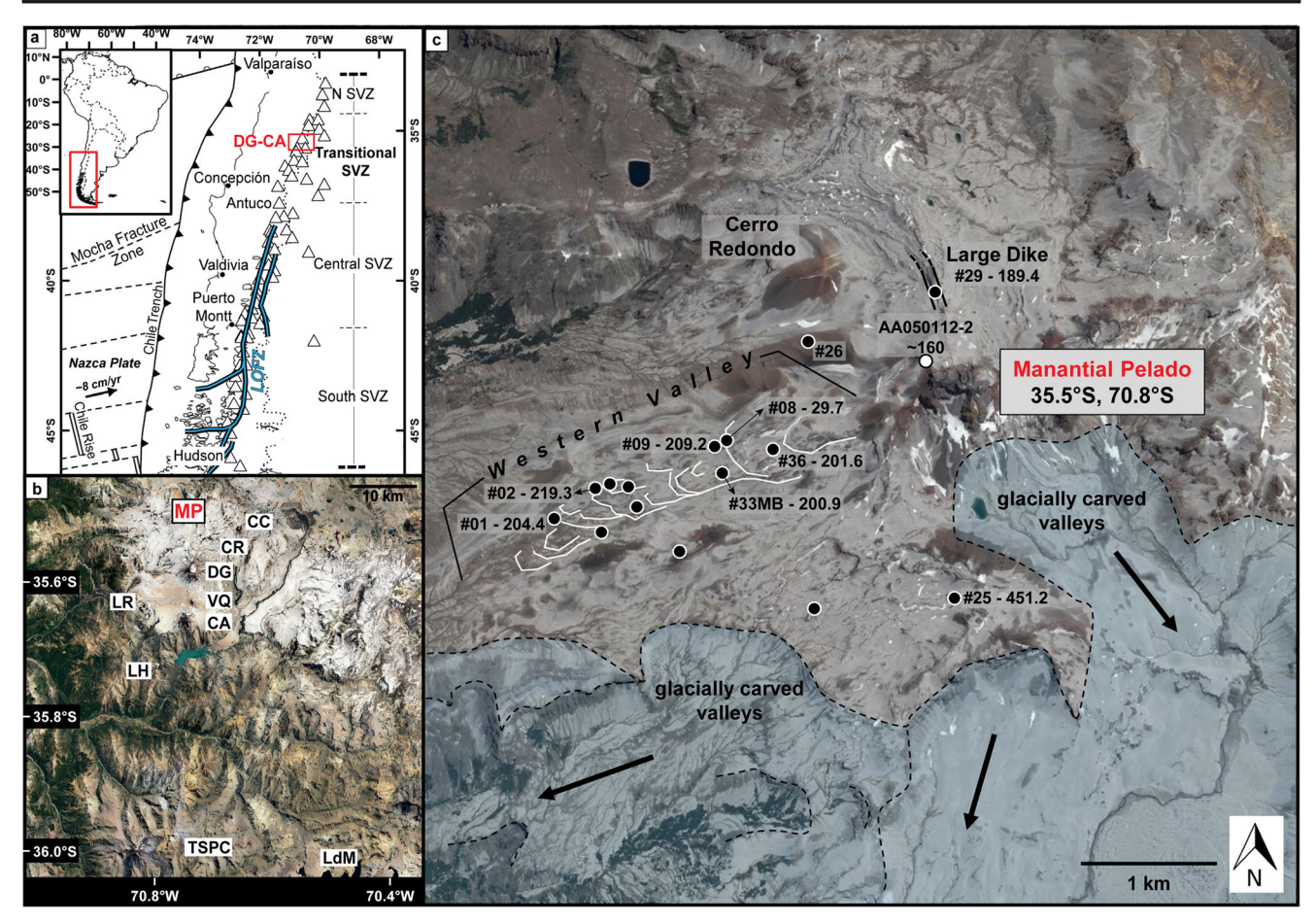


Fig. 1 Overview maps of the Manantial Pelado field area. a Inset map of the Southern Volcanic Zone (SVZ) in Chile broken into four subsequent sections: North, Transitional, Central, and South SVZ. DG-CA denotes the Descabezado Grande-Cerro Azul Volcanic Complex that is in close proximity to Manantial Pelado all within the Transitional SVZ. Blue line: Linquiñe-Ofqui Fault Zone (LOFZ) (Cembrano and Lara 2009). Map modified from Fontijn et al. 2014. b Lower inset map containing the Manantial Pelado field area and surrounding regional volcanic centers. Inset abbreviations: MP Manantial Pelado, CC Cerro Colorado, CR Cerro Rajaduras, DG Descabezado Grande, VQ Volcán Quizapu, CA Cerro Azul, LR La Resolana, LH Los Hornitos, TSPC Tatara-San Pedro,

LdM Laguna del Maule. Imagery was taken from Google Earth. **c** Map of Manantial Pelado field area. Black dot with white rim: sample locations that have undergone bulk-rock analysis. Numbers next to sample location are the specific sample number (#) followed by  $^{40}$ Ar/ $^{39}$ Ar dates in ka (ex: sample #—age date). White dot with black rim: volcanic neck sample location and  $^{40}$ Ar/ $^{39}$ Ar date from SERNAGEOMIN. White lines indicate flow fronts within the Western valley. Pale blue infill highlights some of the main glaciated areas. Note that the blue areas not only show the locations of glaciation but also highlight some of the larger carved valleys. Imagery was taken from Google Earth

crustal thinning (Tassara and Echaurren 2012), Manantial Pelado sits atop an ~45–50-km-thick arc crust. In addition to the overall crustal thinning southward, multiple studies identify smaller volcanic segments within the SVZ based on chemistry and lateral offset, all of which result in four segments: The northern (NSVZ), transitional (TSVZ), central (CSVZ), and southern volcanic zone (SSVZ) (Fig. 1a; López-Escobar et al. 1995; Dungan et al. 2001; Tassara and Echaurren 2012). A major eastward lateral shift at 36° S, just south of Manantial Pelado, separates the TSVZ from the CSVZ and may be caused by the Mocha Fracture Zone projecting underneath the arc (Fig. 1a; López-Escobar et al. 1995; Sellés et al. 2004). The TSVZ that contains Manantial Pelado is comprised of both andesitic and basaltic andesites with true basalts generally lacking. Continental crustal

contributions are still evident at these latitudes through Sr ratios and other geochemical proxies (Grunder 1987; Jacques et al. 2013).

The change in crustal thickness in the SVZ has been leveraged as a natural laboratory for understanding along-arc chemical compositional variability and crustal contributions in many previous studies. Systematic southward decreases in  $\rm K_2O$ ,  $\delta^{18}\rm O$ , and  $\rm ^{87}\rm Sr/^{86}\rm Sr$  and increases in MgO and  $\rm ^{143}\rm Nd/^{144}\rm Nd$  suggest decreasing crustal contributions during magma evolution (Grunder 1987; Hildreth and Moorbath 1988; Stern and Kilian 1996; Rodríguez et al. 2007). These signatures were used to argue for a MASH zone near the lower crust-mantle boundary that leads to overprinting of mantle parentage and the addition of crustal material (Hildreth and Moorbath 1988). More recently, Turner et al. (2016, 2017)



69 Page 4 of 24 Bull Volcanol (2020) 82:69

explored how much compositional diversity may already be imparted through magma generation processes in the mantle. In their model, crustal thickness links directly to the wedge thermal structure, where a thicker overriding crust results in a high pressure-low temperature mantle wedge that decreases the amount of melting and affects chemical compositions and the resulting mineralogy (Turner et al. 2016).

Locally, the TSVZ around Manantial Pelado is volumetrically dominated by silicic systems, such as the Descabezado Grande-Cerro Azul (DG-CA) Volcanic Cluster ~ 10 km to SE of Manantial Pelado (Fig. 1b; Hildreth and Drake 1992; Ruprecht et al. 2012). Aside from Manantial Pelado, only a few other mafic-intermediate centers exist in the TSVZ area. The presumably longer lived systems Cerro Rajaduras and Cerro Colorado have an extensive eruptive history and may be similar to Manantial Pelado; however, they have yet to be studied in detail (Fig. 1b). There are also two short-lived Holocene cinder cone clusters: La Resolana and Los Hornitos (Fig. 1b). Some geochemistry has been reported for both clusters (Ruprecht et al. 2012; Salas et al. 2017), and the latter contains the most primitive magmas in the SVZ (Salas et al. 2017). Here, we compare some of our data to this center.

### Field relations and stratigraphy at Manantial Pelado

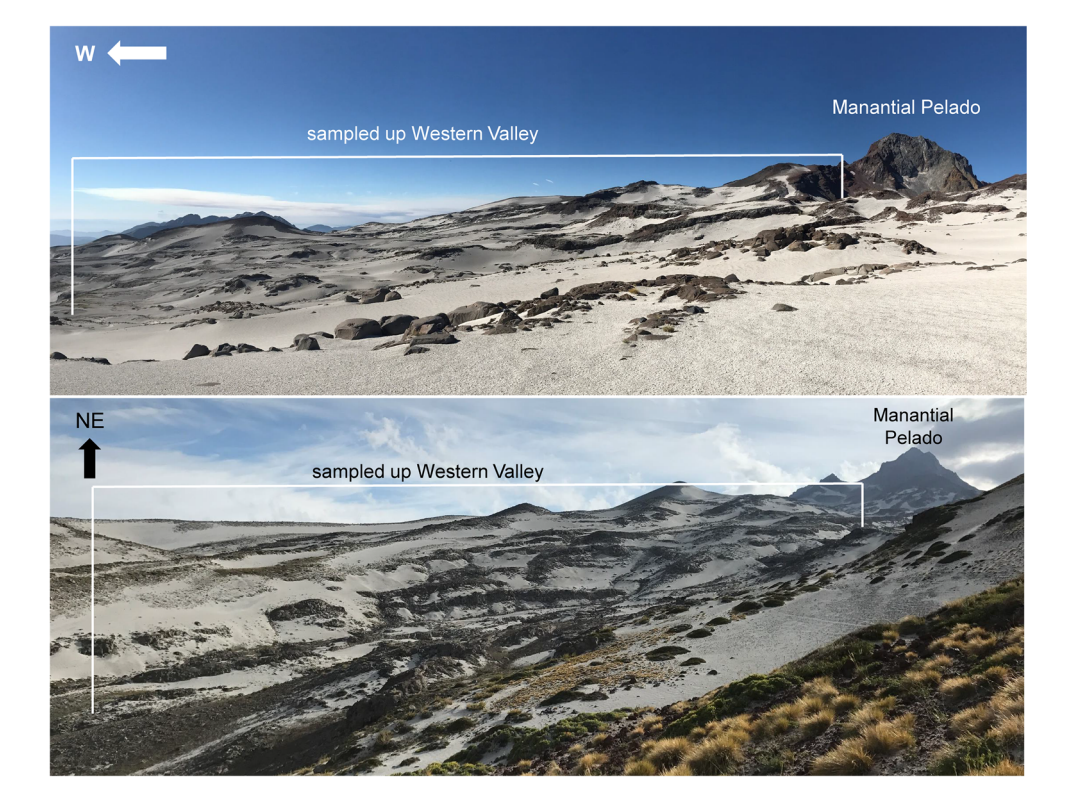
Our field mapping reveals that the Pleistocene volcanic stratocone of Manantial Pelado (3046 m) is dominated by

Fig. 2 Field images of the sampled Western Valley to highlight the extensive nature of basaltic andesite flows. Both images are of the same valley from different angles. Sampling line is  $\sim 2.5$  km

packages of numerous basaltic andesite lavas that are radially exposed in glacially carved valleys extending between 4 and 8 km from the eruptive center (Figs. 1, 2, and 3). The northeastern sector of the volcano is extensively overprinted by hydrothermal activity and the southern sector is partially covered by more recent volcanic activity. In most places, we observed a centimeter-to-decimeter-thick layer of pumice from the 1932 Quizapu eruption that covers the edifice and the surrounding flows (VQ, Fig. 1b; Hildreth and Drake 1992). Near the main edifice, layers of agglutinated and oxidized tephra become more abundant, which we suggest provides evidence for more explosive activity in Manantial Pelado's history. This study focuses on the northwestern to southwestern sector of Manantial Pelado where individual spatially extensive flows (~4–8 km in length, 5–10 m thick) make up thick lava sequences ( $\sim 165$  m thick exposed; Figs. 1, 2, and 3), which are separated by top and basal flow breccias. These sequences show extensive glacial striations on the sequence-capping lava flows.

In addition to the predominance of lava flows, we observed multiple NNW-trending dikes cut through the north side of the volcanic neck (Fig. 1c). One dike is particularly massive ranging in width from  $\sim 5-8$  m (proximal to the volcanic neck) to  $\sim 15-30$  m (distal), and reaches  $\sim 600$  m in length (Figs. 1c, 3, and 4; sample: MP-17-29). The dike marks the eastern boundary for this study.

Approximately  $\sim 1$  km NW of Manantial Pelado sits an  $\sim$  150-m-high oxidized cinder cone: Cerro Redondo (Figs. 1c and 3). Field relations suggest that it is younger than the lava





Bull Volcanol (2020) 82:69 Page 5 of 24 69



Fig. 3 Field photo displaying stacks of basaltic andesite lava flows, Cerro Redondo, and the large dike (MP-17-29). PP Planchón-Peteroa

sequences that dominate the northern and western slopes of Manantial Pelado. Compacted and partially altered tephra deposits from Cerro Redondo are partially preserved on nearby ridges (Fig. 1c). These tephra deposits (MP-17-26, Fig. 1c) are separated from the overlying 1932 Quizapu ash by a paleosol suggesting that significant time had passed after eruptions from Cerro Redondo and the most recent activity at Quizapu (Hildreth and Drake 1992). Moreover, the ridges near Cerro Redondo are covered in sporadic bombs ranging in size from 0.2 to 2 m. Unlike the northern and western slopes of Manantial Pelado, the southern and southwestern sector is more complex. Our field mapping revealed a composite depositional history including the presence of disconformities between lava sequences. This complexity seems to be created by a combination of erosional processes dissecting the landscape and lava emplacement from both Manantial Pelado and Descabezado Grande.

# Fig. 4 Close-up field photo of the large dike cutting into the volcanic neck of Manantial Pelado. Dike is approximately 5–8 m wide

#### Sample collection

A total of 53 samples (49 lavas, two tephra samples, one volcanic bomb, and one dike sample) were collected throughout the stratigraphy on the southern and western flanks (Figs. 1c and 2). Two tephra samples and a volcanic bomb were collected from Cerro Redondo (MP-17-26; Fig. 1c). To obtain constraints on the earliest history of Manantial Pelado, we sampled a flow (MP-17-25) that is older than one of these disconformities, and therefore, it may represent the eruptive character of Manantial Pelado prior to the eruptive phase that produced the extensive lava flows mostly exposed on the western slopes. To fully bracket Manantial Pelado's eruptive history, we also sampled the prominent basaltic andesite dike striking NNW through the volcanic neck (MP-17-29) representing some of the youngest activity (Fig. 1c). We sampled the massive dike as an age-constraint for the volcanic





69 Page 6 of 24 Bull Volcanol (2020) 82:69

Table 1 40 Ar/39 Ar dates of aphyric andesite and basaltic andesite. Further geochronology details and figures are provided in Online Resource D1

| Sample Number | Latitude  | Longitude | Lithology                     | Best age type | Best age | $\pm1\sigma$ |
|---------------|-----------|-----------|-------------------------------|---------------|----------|--------------|
| MP-17-08      | - 35.5107 | - 70.8432 | Aphyric andesite              | Plateau       | 29.7     | 2            |
| AA050112-2*   | -35.5080  | -70.8197  | Basaltic andesite             | Plateau       | 160      | 20**         |
| MP-17-29      | -35.5011  | -70.8183  | Porphyritic basaltic andesite | Plateau       | 189.4    | 6.4          |
| MP-17-36      | -35.5122  | -70.8374  | Porphyritic basaltic andesite | Plateau       | 201.6    | 7.3          |
| MP-17-33MB    | -35.5137  | -70.8456  | Porphyritic basaltic andesite | Isochron      | 200.9    | 26.6         |
| MP-17-09      | -35.5107  | -70.8434  | Porphyritic basaltic andesite | Plateau       | 209.2    | 7.2          |
| MP-17-02      | -35.5133  | -70.8579  | Porphyritic basaltic andesite | Plateau       | 219.2    | 6            |
| MP-17-01      | -35.5148  | -70.8606  | Porphyritic basaltic andesite | Plateau       | 204.4    | 5.8          |
| MP-17-25      | -35.5275  | -70.8219  | Porphyritic basaltic andesite | Plateau       | 451.2    | 5.4          |
|               |           |           |                               |               |          |              |

<sup>\*</sup>SERNAGEOMIN volcanic neck sample

center as it cuts through flows on the north side of the volcano and volcanic neck (Table 1). The disconformable lava (MP-17-25) was collected on the south side of the volcano and is distinct both petrographically and at the outcrop-scale. It is blocky and much thicker (~15 m) than most lavas from Manantial Pelado. While we age-dated the younger dike and older disconformable lava to bracket the eruptive activity, we also age-dated the stratigraphy of basaltic andesite flows that were predominantly erupted and deposited in between the two end-members. Three distinct lithologies were recognized while sampling and will be referenced as follows in decreasing abundance: (1) basaltic andesite, (2) aphyric andesite, and (3) plagioclase andesite. The basaltic andesites are the focus of this study as they dominate the eruptive history and makeup ~ 33 of the 36 sampled flows (Figs. 1, 2, and 3).

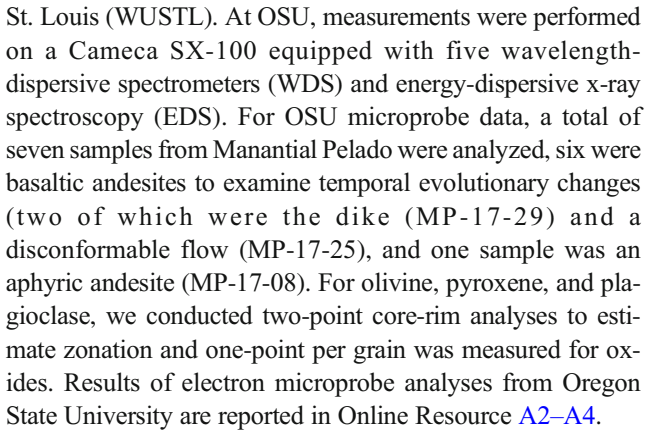
#### **Analytical methods**

#### Whole-rock analyses

X-ray fluorescence (XRF) analyses of 19 whole-rock samples were carried out at the GeoAnalytical Lab at Washington State University (Pullman, WA, USA) following the analytical procedure of Johnson et al. (1999) (Online Resource A1). Inductively coupled plasma mass spectrometry (ICP-MS) analyses were carried out using their high-resolution single collector Finnigan Element2 ICP-MS. One duplicate bead was made to test reproducibility. Unique International Geo Sample Numbers (IGSN) for the analyzed samples are provided in Online Resource A1.

#### Mineral analyses

Mineral chemistry was determined via electron microprobe at Oregon State University (OSU) and Washington University in



High-precision major and trace element (Na, Mg, Al, Si, P, S, K, Ca, Ti, Cr, Mn, Fe, Ni, V) analyses were collected at Washington University in St. Louis using a JEOL JXA-8200 electron microprobe equipped with five WDS, a silicon drift detector (SDD), and EDS. A total of eight samples were analyzed—all of which were basaltic andesites. Two-point core-rim analyses and mineral traverse were performed on olivine, and one-point analyses were performed on oxides in addition to collecting ilmenite-magnetite touching oxide pairs. The results of analyzed olivine, groundmass oxides, and spinel phases from WUSTL are reported in Online Resource A5 and A6.

Olivine Fo zonation profiles were obtained using back-scattered electron (BSE) gray values calibrated to Fo content (Online Resource C1–5). A JEOL 7100FT field emission scanning electron microscope with energy-dispersive x-ray spectroscopy (SEM-EDS) at the University of Nevada, Reno, was used to measure Fo content across each olivine grain (4–9 spots per grain). Those analyses were used to calibrate BSE gray values to Fo content. Major element point analyses agree with electron microprobe analyses. Major element uncertainties of the calibrated olivine BSE images are primarily affected by the uncertainties in the spot



<sup>\*\*</sup>Error at 2σ

Bull Volcanol (2020) 82:69 Page 7 of 24 69

measurements (typically < 0.5 mol units) as the calibration curves have reported  $R^2$  values  $\geq 0.99$  (Online Resource C1-5).

#### Geochronology

Dating of eight samples using the 40Ar/39Ar method was carried out at the United States Geological Survey (USGS) in Menlo Park, CA, to constrain the timing and duration of magmatism at Manantial Pelado. Samples cover the entire stratigraphy in the studied valleys (Figs. 1 and 2). Groundmass separates from each sample were prepared for dating via the 40Ar/39Ar method. Samples were crushed, ultrasonicated, and sieved to 200 to 425 µm. Groundmass was separated from phenocryst phases using a Frantz magnetic separator and careful handpicking under a binocular microscope. Approximately 100 to 150 mg of material was prepared for each groundmass separate. Groundmass separates were packaged in Al foil along with Bodie Hills sanidine monitor minerals (9.7946 ± 0.0031 Ma, equivalent to Fish Canyon sanidine at  $28.099 \pm 0.013$  Ma; Fleck et al. 2019) and encapsulated in quartz vials. The quartz vials were wrapped in 0.5mm-thick Cd foil to shield samples from thermal neutrons during irradiation. Samples were irradiated for 1 h in the central thimble of the USGS TRIGA reactor in Denver, CO (Dalrymple et al. 1981) at a power level of 1 MW. Following irradiation, the samples were rewrapped in degassed Ta foil prior to analysis. For incremental heating analysis of groundmass separates, the argon was extracted in 9 to 15 discrete temperature steps using a diode laser attached to a MAP 216 mass spectrometer at the USGS in Menlo Park, CA. Temperatures were monitored using an optical pyrometer. Prior to measurement of Ar isotopic composition, groundmass separates were degassed at 400 °C until undesirable gases (e.g., water, nitrogen, and hydrocarbons as measured by a Granville-Phillips 835 VQM) were reduced to acceptable levels. For all experiments, extracted Ar was exposed to a 4-A tungsten filament, 125 K cold finger, and two SAES ST-175 getters (one operated at 300 °C and one at room temperature) to remove active gasses. <sup>40</sup>Ar/<sup>39</sup>Ar ages are calculated using the decay constants recommended by Steiger and Jäger (1977). Uncertainties in reported sanidine <sup>40</sup>Ar/<sup>39</sup>Ar ages include propagated uncertainties in counting statistics and J values. Instrumental mass discrimination was calculated by repeated measurement of atmospheric argon, assuming  $^{40}$ Ar/ $^{36}$ Ar<sub>atmosphere</sub> = 298.56 ± 0.31 (Lee et al. 2006). See Calvert and Lanphere (2006) and Fleck et al. (2014) for additional details regarding analytical techniques, mass spectrometer design, and irradiation procedures.

We also report an age for the volcanic neck produced by the Chilean Servicio Nacional de Geología y Minería (SERNAGEOMIN; sample: AA050112-2). The <sup>40</sup>Ar/<sup>39</sup>Ar geochronological dating was carried out at the Isotope Geology Laboratory of SERNAGEOMIN on groundmass. Approximately 1 kg of sample was crushed and sieved to obtain grain sizes of 100-250 µm. Groundmass was separated from phenocryst phases using an isodynamic Frantz magnetic separator and heavy liquids, followed by handpicking under binocular microscope. Samples were mounted on high-purity Al discs, together with sanidine crystals of Fish Canyon standard sample ( $28.02 \pm 0.1$  Ma; Renne et al. 1998). Samples were irradiated in a RECH-1 nuclear reactor at CCHEN (Comisión Chilena de Energía Nuclear, La Reina, Santiago) nuclear reactor facility for 22 h in a Herald-type pool, at 5 MW. Samples inside the reactor were mounted in a stable and rotating position, surrounded by a Cd shell. The rotating system was used to obtain a homogeneous J factor for the various samples across the disk. After irradiation, the samples were placed on a copper disc with a potassium bromide cover and mounted in the sample chamber of the sample zone of the spectrometer, under ultrahigh-vacuum conditions. Samples were heated by successive power steps induced by a CO<sub>2</sub> laser with a maximum energy of 30 W. Every three analytical steps, blank measurements were made, to correct successive measurements. Noble gases extracted from the sample were separated using a cold finger trap and one getter (ST101), operated at 2.2 A. Purified sample was introduced in the MAP 215-50 mass spectrometer. Isotope contents for masses <sup>36</sup>Ar, <sup>37</sup>Ar, <sup>38</sup>Ar, <sup>39</sup>Ar, and <sup>40</sup>Ar were measured using a high-resolution electron multiplier, together with baseline measurements for every heating step. The apparent ages obtained for every heating step take into account corrections for interference of isotopes generated during irradiation from K, Ca, and Cl. The criterion for defining a "plateau age" corresponds to three or more successive steps overlapping with an error at  $2\sigma$  level and containing > 50% of released <sup>39</sup>Ar (Fleck et al. 1977). The decay constant for 40K used for calculations is that proposed by Steiger and Jäger (1977). The atmospheric ratio for  $^{40}$ Ar/ $^{36}$ Ar<sub>atmosphere</sub> is assumed to be 295.5 ± 0.5. It should be noted that the samples collected for <sup>40</sup>Ar/<sup>39</sup>Ar geochronological dating at the USGS and the sample of the volcanic neck dated by the SERNAGEOMIN were prepared in different labs and with slightly different techniques.

#### **Results**

#### Lithologic description

We have grouped Manantial Pelado lavas into three distinct lithologies: olivine-plagioclase porphyritic basaltic andesite (referred to as basaltic andesite), nearly aphyric andesite, and plagioclase andesite (also referred to as evolved andesite). Majority of the flows on the western flank of the volcano are basaltic andesite. Higher up on the edifice (and presumably later in Manantial Pelado's history; Table 1), aphyric and



69 Page 8 of 24 Bull Volcanol (2020) 82:69

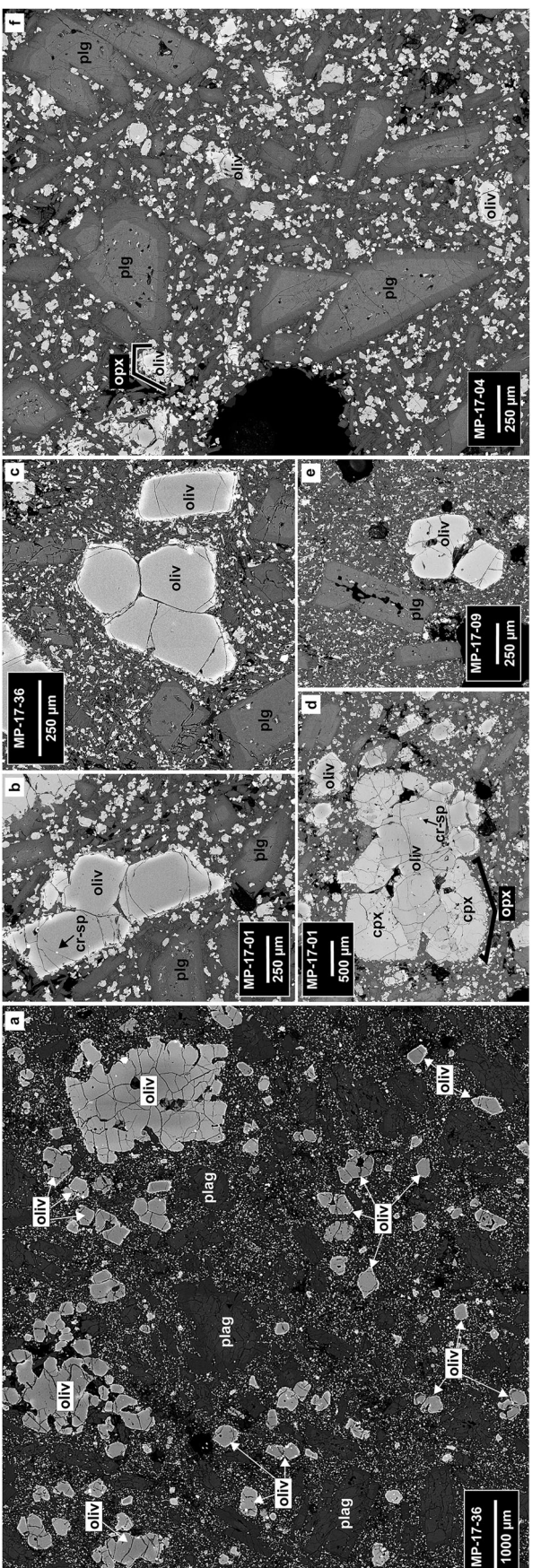


Fig. 5 Back-scattered electron images of samples to display crystal textures, groundmass, and zonations patterns. a Sample MP-17-36 edited to highlight olivine textures. Cr-spinel identified within olivine cores. Large phenocrysts (1–2 mm) could represent evidence this system is not fully closed and has olivine cores which have been inherited from other pre-existing crystal-mush domains, or the large phenocrysts could represent potential xenocrysts. They are not prevalent

throughout all flows, but are present in this sample. Original image can be found in Online Resource B1. b Olivine crystals with flat cores and cr-spinel inclusions. c Olivine crystals with flat cores. d Evidence of olivine-clinopyroxene glomerocrysts and orthopyroxene overgrowth. e Plagioclase resorption texture and melt inclusion evidence. f Displays plagioclase zonation patterns and orthopyroxene overgrowth texture



Bull Volcanol (2020) 82:69 Page 9 of 24 69

plagioclase-andesites are exposed above the basaltic andesite lavas, documenting compositional variation within close spatial proximity (Online Resource B2). Aphyric andesites are always found as isolated flows with a depositional contact overlying basaltic andesite lavas. Plagioclase andesite lavas are typically found up sequence from the aphyric andesite. Neither of these two lithologies have basaltic andesites emplaced on top of them.

Tephra, presumably from Cerro Redondo, was sampled on an exposed ridge NW of Manantial Pelado, where we excavated an  $\sim 1.5$ -m-thick section (the bottom was not reached). We identified two distinct layers that alternate between larger clast sizes ( $\sim 2-3$  cm) to finer clasts ( $\sim 0.5-1$  cm). Our stratigraphic section was topped with ~5 cm of fine ash presumably from the 1932 Quizapu eruption that was directly underlain by a thin (0.5–1 cm) paleosol layer. The following layer underlying the paleosol was an ~50-cm-thick, crystal-poor, vesiculated black scoria tephra section with grain sizes ranging from 0.5 to 3 cm (MP-17-26b). The following tephra section was ~ 20-cm-thick, crystal-poor, vesiculated black scoria layer ranging in size from 0.5 to 1 cm (MP-17-26a). The lowermost layer observed in our stratigraphic section was ~ 75 cm thick (bottom not exposed) and of similar size and composition to MP-17-26b.

#### **Petrographic description**

Basaltic andesites are the dominant lithology throughout Manantial Pelado's eruptive history. The phase assemblage, in order of abundance, consists of phenocrysts of calcic-plagioclase, olivine, clinopyroxene, and microphenocrysts and microlites of mostly orthopyroxene and sodic-plagioclase in the groundmass (Fig. 5, Online Resource B1). Plagioclase phenocrysts are euhedral (occasionally subhedral) and range from 1 to 2 mm in size. Plagioclase zoning patterns and textures are variable with predominantly normal zonation to occasional reverse zonation. Some grains have sieved cores and/ or growth zones with abundant melt inclusions. Olivine is the most abundant mafic phase with phenocrysts ranging in size from 0.5 to 1 mm, but can be as large as 2-3 mm that are subhedral to euhedral in shape (Fig. 5). Olivine cores are generally unzoned with spinel inclusions. Olivine rims are normally zoned and frequently overgrown by narrow orthopyroxene rims (~10 μm wide) (Fig. 5). Clinopyroxene is the least abundant phenocryst phase (1-3 mm) and occasionally forms glomerocrysts with olivine (Fig. 5). The holocrystalline groundmass (crystals < 150 μm) consists of plagioclase, orthopyroxene, pigeonite, and Fe-Ti oxides (predominantly titanomagnetites) with slight trachytic textures around large phenocrysts (Fig. 5). We estimate that the Manantial Pelado basaltic andesites are ~45–55% crystalline based on image analysis using JMicroVision randomized point-counting with uncertainties of  $\sim 5\%$  based on counting statistics. Crystallinity was estimated for phenocrysts >  $100 \mu m$ , which excludes microlites, and the lavas are dominated by olivine and plagioclase with subordinate pyroxene and spinel. Manantial Pelado crystallinity is considered a maximum estimate as the point-counting included zoned phenocryst rims that could represent late-stage growth.

We have identified a sub-group within the basaltic andesite lithology termed texturally uncommon basaltic andesites that tend to be more evolved than the standard basaltic andesite samples. While the dominant basaltic andesite samples were sampled up glacially carved valleys in stratigraphic succession, this sub-group of samples contains a variety of samples: the oldest end-member flow (MP-17-25), a spindle bomb (MP-17-26c) and tephra (MP-17-26a-S1) from Cerro Redondo, an unusual flow with enclaves of the standard basaltic andesite composition (MP-17-22b-e), and a flow that directly overlies the apyhric andesite (where other identified aphyric andesite is consistently the highest, most recent stratigraphic flow; MP-17-09).

The nearly aphyric andesite contains minor, commonly acicular plagioclase ( $\sim 1-2\%$ ; 1–6 mm; Online Resource B2). Olivine is rare ( $\ll 1\%$ ), but when present, it occurs in clusters of anhedral crystals. Apatite occurs as an accessory phase. The third lithology, plg-porphyritic andesite, contains plagioclase (2–4%, < 1–3 mm) and is commonly found above the aphyric andesite with no contact exposed.

#### Chronostratigraphy

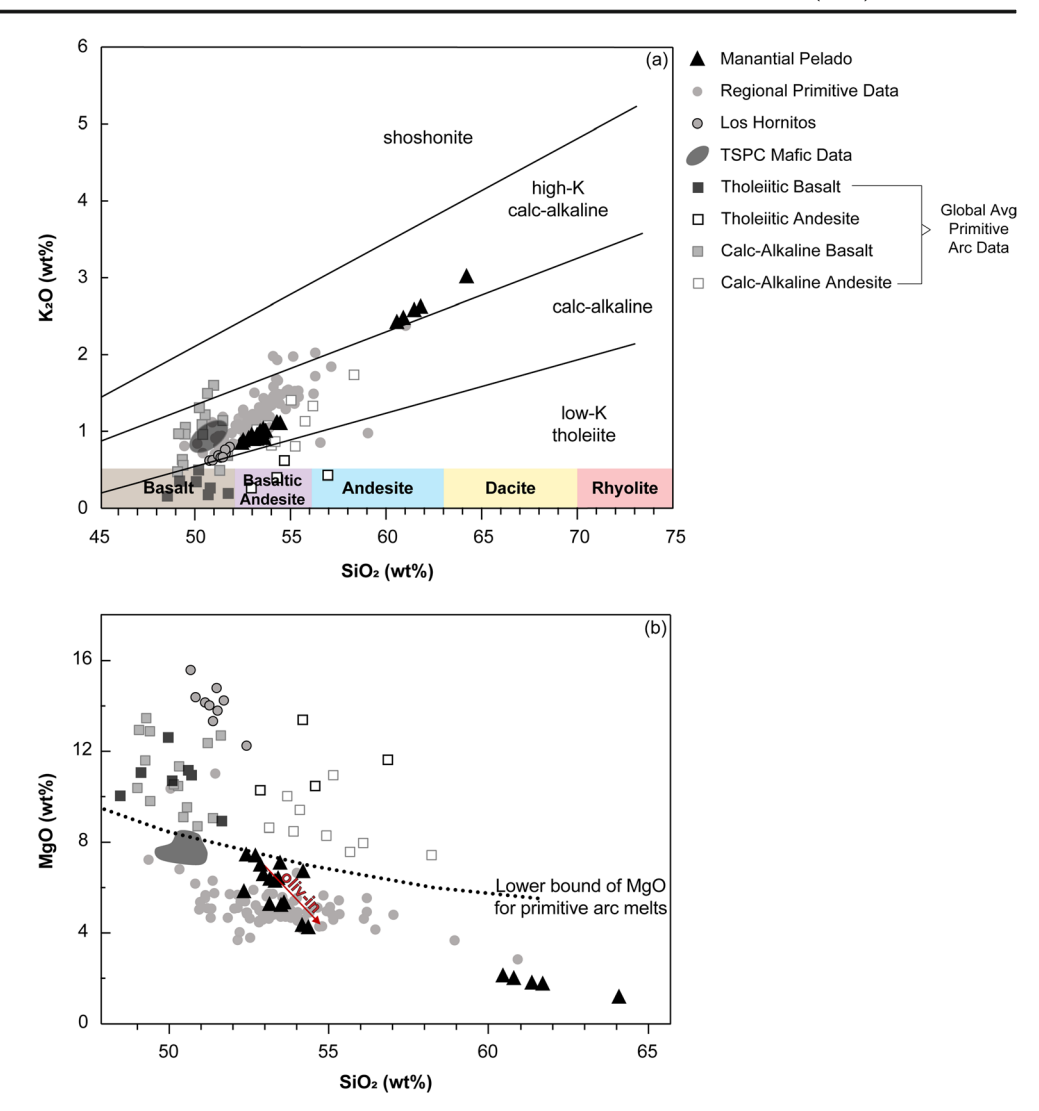
Dates for seven basaltic andesite lavas and one aphyric andesite lava (MP-17-08) yield Pleistocene ages (Table 1). The two samples that bracket most of Manantial Pelado's eruptive history are the disconformably overlain lava (MP-17-25;  $451.2 \pm$ 5.4 ka) and the major NNE-trending dike (MP-17-29; 189.4  $\pm$ 6.4 ka). Flows found in stratigraphic succession within the western valley (Figs. 1 and 2) range in age from ~200 to 219 ka. These flows are also listed in stratigraphic order within Table 1. Sample MP-17-01 (204.4  $\pm$  5.8 ka, at  $1\sigma$  error) was deposited at the very base of the exposed flows, and therefore, based on field relations, it is the oldest in the sequence. Five of the lava flows from the western portion of Manantial Pelado have <sup>40</sup>Ar/<sup>39</sup>Ar ages within analytical error of each other, yielding a weighted mean age of  $209 \pm 6.3$  ka  $(2\sigma)$ ; MSWD = 1.16). This indicates that all of these lavas erupted over a short time interval < 20 kyr. The aphyric andesite (MP-17-08) gave an  $^{40}$ Ar/ $^{39}$ Ar age of 29.7 ± 2 ka. The exposed depositional contact of the dated aphyric andesite overlaying basaltic andesite initially suggests an abrupt compositional change; however, the significantly younger age of the aphyric andesite implies other scenarios are more likely and will be discussed in more detail later.

The age provided by SERNAGEOMIN for the volcanic neck is  $\sim 160 \pm 20$  ka (Table 1; Fig. 1c; Sample: AA050112-



69 Page 10 of 24 Bull Volcanol (2020) 82:69

Fig. 6 a Subdivision of subalkaline rocks from XRF data. Rock type fields are based on the IUGS classification scheme from Le Maitre et al. (2002). Samples display primarily calc-alkaline characteristics. Olivine-bearing basaltic andesite plots near tholeiitic compositions. b MgO vs SiO<sub>2</sub> plot (XRF data). Dotted line: lower bound of MgO for global primitive arc melts (Schmidt and Jagoutz 2017). Manantial Pelado data plots exactly at lower bound for primitive arcs and displays the highest primitive signatures with TSPC compared with regional data. Black triangle: Manantial Pelado. Dark gray polygon: Mafic data from Tatara-San Pedro (Jweda 2014). Gray dot: regional primitive data (primitive centers near Laguna del Maule, Laguna del Maule, Nevados de Longavi, Los Hornitos/Cerro Azul, cones related to TSPC; Hildreth et al. 2010; Jacques et al. 2013; Wehrmann et al. 2014a). Gray dot/black rim: Los Hornitos (Salas, in review). Squares: Global average primitive arc data (Schmidt and Jagoutz 2017). Light gray-filled square: calcalkaline basalts. Light grayoutlined square: calc-alkaline andesite. Dark gray-filled square: tholeiitic basalt. Dark grayoutlined square: tholeiitic andesite



2). It may represent the final activity of the central vent concluding the phase of dominant basaltic andesite eruptions. The age is consistent by being slightly younger than the dike sample, but it is significantly older than the aphyric andesites.

#### Whole-rock data

Bulk-rock compositions of lavas range from 52 to 64 wt% SiO<sub>2</sub> and 1 to 7.5 wt% MgO (Online Resource A1). A compositional gap separates the basaltic andesite from the andesite lava (54–61 wt% SiO<sub>2</sub>; 2–4 wt% MgO; Fig. 6). Basaltic andesites are restricted to 4–7.5 wt% MgO, Mg#<sub>55–70</sub>, 30–85 ppm Ni, where the evolution among the basaltic andesites is consistent with olivine fractionation and Ni depletion (Figs. 6 and 7; Mg# calculated on molar basis ((Mg/(Mg + Fe)\*100)). At 2 wt% MgO, Ni flattens out while MgO continues to decrease (Fig. 7). FeO\* increases until ~4–5 wt% MgO and is followed by a decrease due to Fe-oxide

crystallization.  $TiO_2$  increases until 4 wt% MgO and begins to decrease at 2 wt% MgO. Initial enrichment within the basaltic andesite suggests Ti-oxide suppression until 2 wt% MgO where ilmenite or titanomagnetite start to crystallize (Online Resource B3). At ~5 wt%, MgO, CaO, and Sc contents drastically decrease indicating clinopyroxene fractionation that could co-crystallize with plagioclase (Online Resource B3; Gavrilenko et al. 2016). The fact that plagioclase and pyroxene potentially join the liquidus is supported by  $Al_2O_3$  and Sr plots which show initial enrichment followed by depletion also at ~5 wt% MgO (Online Resource B3).

Trace element abundances of Manantial Pelado basaltic andesites display typical subduction zone characteristics (Fig. 8, Online Resource A1) with enrichment in large ion lithophile elements (LILE) and depletion in high-field strength elements (HFSE). The basaltic andesites show no Eu anomaly (Eu/Eu\*  $\sim$  1) and the onset of Sr and Al $_2O_3$  depletion through plagioclase crystallization is only evident for more evolved



Bull Volcanol (2020) 82:69 Page 11 of 24 69

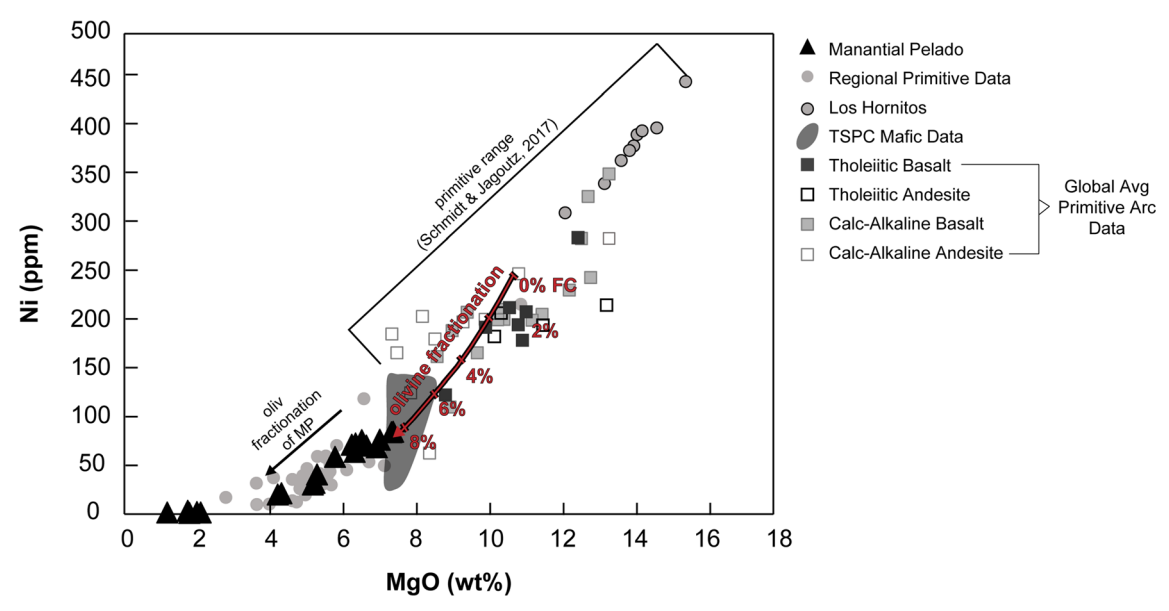


**Fig. 7** Ni (ppm) vs MgO (wt%) XRF whole-rock data. Black bracket indicates primitive composition based on Schmidt and Jagoutz (2017). Manantial Pelado (MP) data sits at the primitive end-member for regional SVZ primitive centers aside from Los Hornitos. Globally, MP is near-primitive yet not fully to the primitive extent of other centers. About 4–8.5% of olivine fractionation (arrow, see main text for calculation) are required to change a primitive magma composition (150–250 ppm Ni) to the observed compositions in Manantial Pelado basaltic andesites. Black triangle: Manantial Pelado. Dark gray polygon: Mafic data from Tatara-

San Pedro (Jweda 2014). Gray dot: regional primitive data (primitive centers near Laguna del Maule, Laguna del Maule, Nevados de Longavi, Los Hornitos/Cerro Azul, cones related to TSPC; Hildreth et al. 2010; Jacques et al. 2013; Wehrmann et al. 2014b). Gray dot/black rim: Los Hornitos (Salas, in review). Squares: global average primitive arc data (Schmidt and Jagoutz 2017). Light gray—filled square: calc-alkaline basalts. Light gray—outlined square: calc-alkaline andesite. Dark gray—filled square: tho-leiitic andesite

compositions (Fig. 8, Online Resource B3). The strong depletion of Sr in Fig. 8 point towards plagioclase fractionation (Drake and Weill 1975; James 1982). Manantial Pelado plots near other regional (SVZ) and global primitive centers (Online Resource B4). The more evolved lavas are generally more enriched with the exception of elements affected by plagioclase fractionation (e.g., Sr, Eu; Fig. 8, Online Resource B4, B5). One aphyric andesite displays P depletion potentially indicating apatite fractionation (Fig. 8). The evolved andesite compositions display typical fractionation trends away from the near-primitive basaltic andesite with some influence from interaction with crustal rocks or mantle heterogeneity (Figs. 8 and 9; Turner et al. 2017). We observe that the evolved andesites are more enriched in more incompatible elements and have steeper REE patterns than the basaltic andesite (Fig. 8; Online Resource B4, Online Resource B5). These differences are small and most pronounced for Rb and Cs (Online Resource B5), but they indicate that while fractionation of basaltic andesite is likely the dominant process to produce the evolved andesites, some interaction with crustal rocks are likely to contribute to the formation of the evolved andesites. Highly and moderately incompatible trace element ratios also point towards minimal crustal melting effects (Fig. 9). Low Rb/Sr and Ba/La favor plagioclase crystallization and conflict with significant crustal melting (Fig. 9; Hawkesworth et al. 1982; Conrey et al. 2001). Increased crustal melting effects would increase the incorporation of highly

incompatible elements (Rb, Ba) and point towards phases such as potassium-feldspar (Hawkesworth et al. 1982; Conrey et al. 2001). We acknowledge the evolved andesite displays an enriched trend in Fig. 9a, suggesting some crustal interaction in evolved samples; however, if crustal melting played a significant role in the basaltic andesite, we would see positive trends in both Fig. 9 a and b. In fact, Fig. 9b displays relatively flat-to-negative trends towards the evolved andesite and away from crustal signatures.

In addition to the differences between the lithological groups, there is a compositional range within each lithological group. The basaltic andesites display a clear subgrouping with the majority of the basaltic andesites being a tight compositional cluster (denoted by a solid black line in Fig. 8). These basaltic andesites represent the dominant material produced in Manantial Pelado's eruptive history. Other rare samples were observed in the field and classified as texturally uncommon basaltic andesite and are grouped with the basaltic andesites, but they are generally slightly more evolved (Fig. 8).

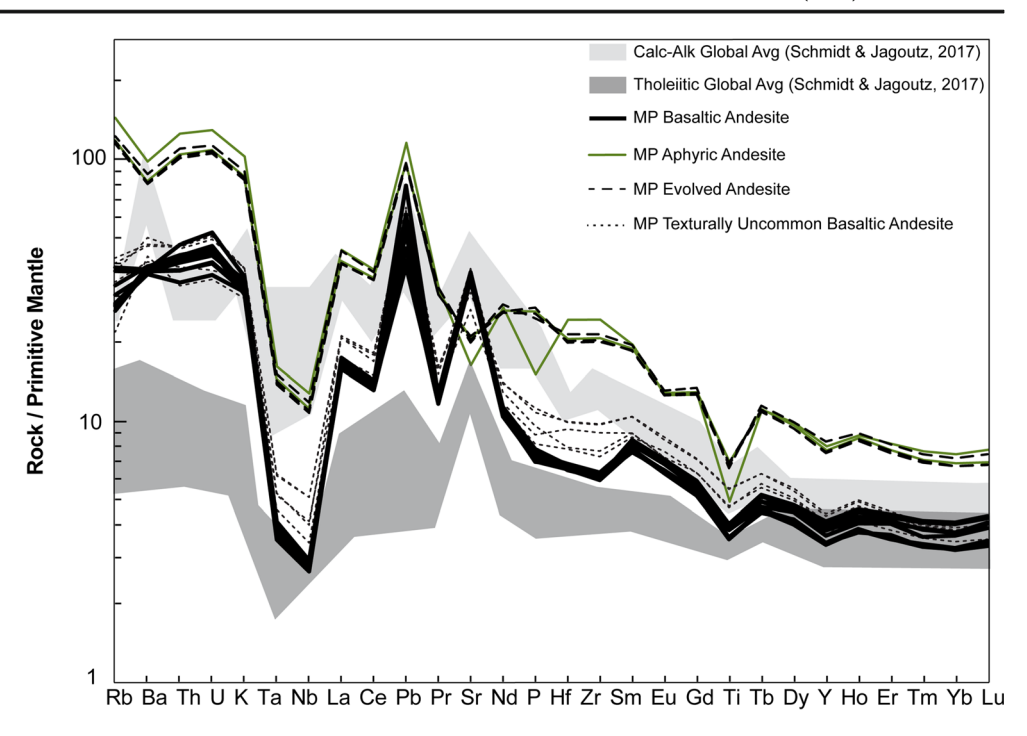
#### Mineral composition

Olivine was analyzed in eight basaltic andesites (Online Resource A5) with core and rim compositions ranging Fo $_{67-87.6}$  and Fo $_{60-79}$ , respectively. Most olivine cores scatter around Fo $_{80-84}$  and Ni content ranges from 195 to 2148 ppm



69 Page 12 of 24 Bull Volcanol (2020) 82:69

Fig. 8 Spider diagram of Manantial Pelado (ICP-MS data) distinguishing differences in lithologies. Normalized to primitive mantle (McDonough and Sun 1995). Black solid line: Manantial Pelado basaltic andesite. Green solid line: Manantial Pelado aphyric andesite. Dashed line: Manantial Pelado evolved andesite. Dotted line: Manantial Pelado texturally uncommon basaltic andesite. Light gray field: global averages for calc-alkaline samples (Schmidt and Jagoutz 2017; Mexico, Cascades, and SVZ calkalkaline basalts). Dark gray field: global averages for tholeiitic samples (Schmidt and Jagoutz 2017; SVZ tholeiitic and Cascades tholeiitic basalt)



(Online Resource A5). Olivine-hosted spinel inclusions are commonly Cr-spinel with the majority having Cr#50. Crspinel crystallizes early while Cr contents are high and melts are primitive (Clynne and Borg 1997; Kamenetsky et al. 2001). Pyroxenes were analyzed in six basaltic andesites that contain mostly clinopyroxene (Mg#<sub>~68-83</sub>) and occasional orthopyroxene and pigeonite were observed within the groundmass (identified qualitatively using SEM). Additionally, the Cr<sub>2</sub>O<sub>3</sub> content within clinopyroxene (> 0.3–0.4 wt%) is at primitive to near-primitive concentrations for calc-alkaline clinopyroxene (Conrad and Kay 1984). Plagioclase (Online Resource A4) phenocrysts are dominated by calcic cores (An $_{\sim 75-89}$ ), while phenocryst rims and microlites in the groundmass are more sodic (An<sub>~46</sub>). The aphyric andesite contained ~ 1-2% phenocrysts with plagioclase sodic cores (An $_{\sim 43-54}$ ) overlapping the rim compositions of more primitive samples.

#### Discussion

## Basaltic andesite and their connection to primitive magmas

The chemical characteristics of Manantial Pelado basaltic andesites suggest only minor evolution from primitive arc magma compositions and can be considered "near-primitive" when compared regionally and globally with primitive compositions. The basaltic andesites consistently plot at the lower bound of primitive compositions (Figs. 6 and 7) taken from the global compilation of Schmidt and Jagoutz (2017). A

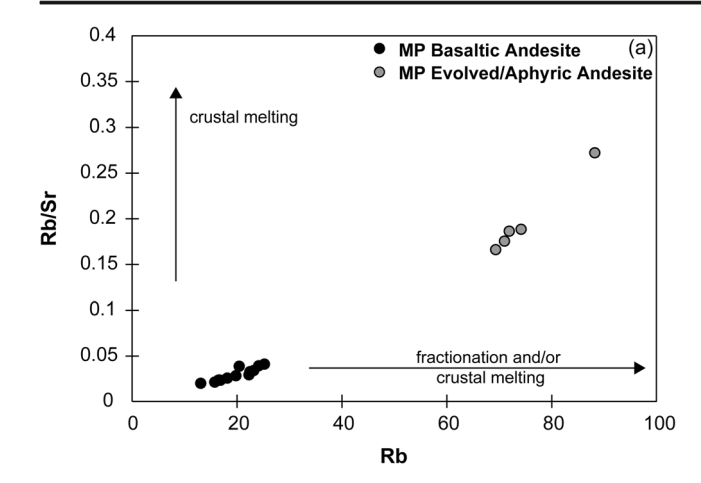
regional comparison of Manantial Pelado magmas to volcanic centers in the SVZ (34° S–41° S, Fig. 10) reveals that Manantial Pelado compositions are among the most primitive in the SVZ (excluding cinder cones) with regard to MgO, SiO<sub>2</sub>, and Ni (Fig. 10a–c). Here the magma compositions for each volcanic center are taken from comprehensive studies of individual volcanoes and along-arc and across-arc compilations (Jacques et al. 2013; Jweda 2014; Turner et al. 2016; Turner et al. 2017) and from the EarthChem Database (see references in Fig. 10). Some of these volcanoes are built on much thinner crust (~36–41° S; Hildreth and Moorbath 1988; Tassara and Echaurren 2012; Turner et al. 2016) which can result in diminished crustal interaction.

The role of the thicker crust at the latitude of Manantial Pelado (35.5° S) and northward remains a highly debated part of the arc. On the one hand, magma staging in the lower crust may contaminate any mantle signature through MASH processes (Hildreth and Moorbath 1988), while alternatively, mantle heterogeneities combined with lower degrees of melting (due to a smaller asthenospheric mantle wedge underneath the thick crust) may be the principle driver for the signatures in mafic magmas (Turner et al. 2016). Thirdly, primitive magma variations may be driven by changes in slab input (Jacques et al. 2014).

A fundamental change in along-arc variations of the SVZ for <sup>87</sup>Sr/<sup>86</sup>Sr occurs between 34 and 36° S. Manantial Pelado is among a cluster of volcanoes at the southern end of this transition along with Planchón-Peteroa, Descabezado Grande, Tatara-San Pedro, and Longavi. To the north, substantially elevated <sup>87</sup>Sr/<sup>86</sup>Sr isotope compositions exist (up to <sup>87</sup>Sr/<sup>86</sup>Sr ~ 0.7056) compared with a relatively confined



Bull Volcanol (2020) 82:69 Page 13 of 24 69



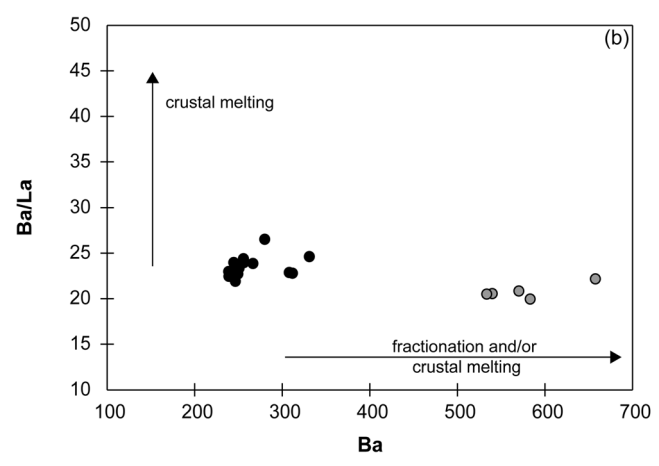


**Fig. 9** Highly and moderately incompatible trace element ratios (ICP-MS data). **a** Rb/Sr vs Rb displays minimal crustal melting signatures for the evolved andesite and relatively low ratios for the basaltic andesite. **b** Ba/La vs Ba displays a relatively flat-to-negative trend away from crustal melting signatures even for evolved andesite

isotope signature of  $^{87}\text{Sr}/^{86}\text{Sr} \sim 0.704$  in the south (Hildreth and Moorbath 1988; Turner et al. 2017). This change may indicate that crustal effects are coupled nonlinearly with crustal thickness. MASH-type processes become inevitable for continental crust greater than  $\sim 50$  km with residual basalt liquids and crustal melts coexisting for thousands of years (Dufek and Bergantz 2005). For thinner crust, melting and assimilation are subordinate, while storage and homogenization of mantle-derived melts may still overprint crystal and textural records and mask the presence of primitive magmas (see below). Manantial Pelado resides at  $\sim 45-50$ -km-thick crust positioning itself on the boundary between these two end-member processes.

While whole-rock compositions from Manantial Pelado cannot completely resolve which mechanism plays a larger role in arc variation for this transitional segment, incompatible trace element ratios can provide initial insight. In Fig. 10d, we place Manantial Pelado in the context of other regional volcanic centers that display positive correlations between La/Sm

and Nd<sub>6.0</sub> (Turner et al. 2016). The positive correlation also reflects along-arc variation as the northern volcanic centers (PP, MP, DG, TSPC, LV) cluster at the highest extent of the trend while the southern centers progressively shift towards lower values (Fig. 10d). This suggests crustal thickness, which correlates with latitude in the SVZ, can account for along-arc geochemical variation. As a response to crustal thickening from south-north, Fig. 10 d highlights the degree of melting decreases moving northward. This characteristic was used to argue that thicker crust induces lower degrees of melting due to a smaller asthenospheric mantle wedge (Turner et al. 2016). Turner et al. (2016, 2017) suggests that along-arc variations are dominantly controlled by mantle heterogeneity and degree of melting with minimal variability resulting from sediment or slab input. Alternatively, sediment or slab input was previously argued to be important by Jacques et al. (2014) on the basis of fluid-mobile elements and isotope compositions. To test whether sediment input may play a fundamental role in the SVZ, we use the widely used sediment tracer of Th/ La relative to Sm/La to explore the variability in a mantle plus altered oceanic crust component (Fig. 10e; Plank 2005). Recent cores from the Ocean Drilling Program (ODP) offshore the Chilean Andes (ODP 1234, ~36° S; ODP 1232, ~ 40° S) were compiled in the global database for subducting sediments (Plank 2014) and represent an excellent endmember for the major arc volcanoes of the SVZ (Fig. 10e). New data from Manantial Pelado display high Th/La and substantiate a mixing relationship for the arc magmas between sediment and a mantle plus altered oceanic crust component. In fact, the high Th/La for Manantial Pelado suggests that variations from slab input may have been underappreciated for this region of the SVZ. Furthermore, variations on the basis of La/Sm (Fig. 10d) are small compared with variations in Th/La (Fig. 10e), and therefore, mantle heterogeneities may be subordinate compared with the influences of slab input. While our data does not resolve the long-standing debate of primitive magma generation in the Southern Andes, we suggest that isotope data for Manantial Pelado and other mafic centers (e.g., Cerro Rajaduras, Cerro Colorado) in this transitional segment of critical crustal thickness are needed to unravel the effects of thick crust and potential variations in mantle chemistry and slab input.

Thus, we argue that in general, Manantial Pelado basaltic andesites can be used to explore processes in the SVZ crust that create the baseline compositions from which other magmas may have evolved. Unlike most other systems in the SVZ (mainly further north), Manantial Pelado basaltic andesites show minimal overprinting by crustal processes, such as mixing and assimilation, based on major and trace elements (Hildreth and Moorbath 1988) and preserve much of the initial compositions prior to their evolution. Additionally, the high contents of MgO (7.4 wt%), Ni (86 ppm), and corresponding Mg# up to ~68 argue that



69 Page 14 of 24 Bull Volcanol (2020) 82:69

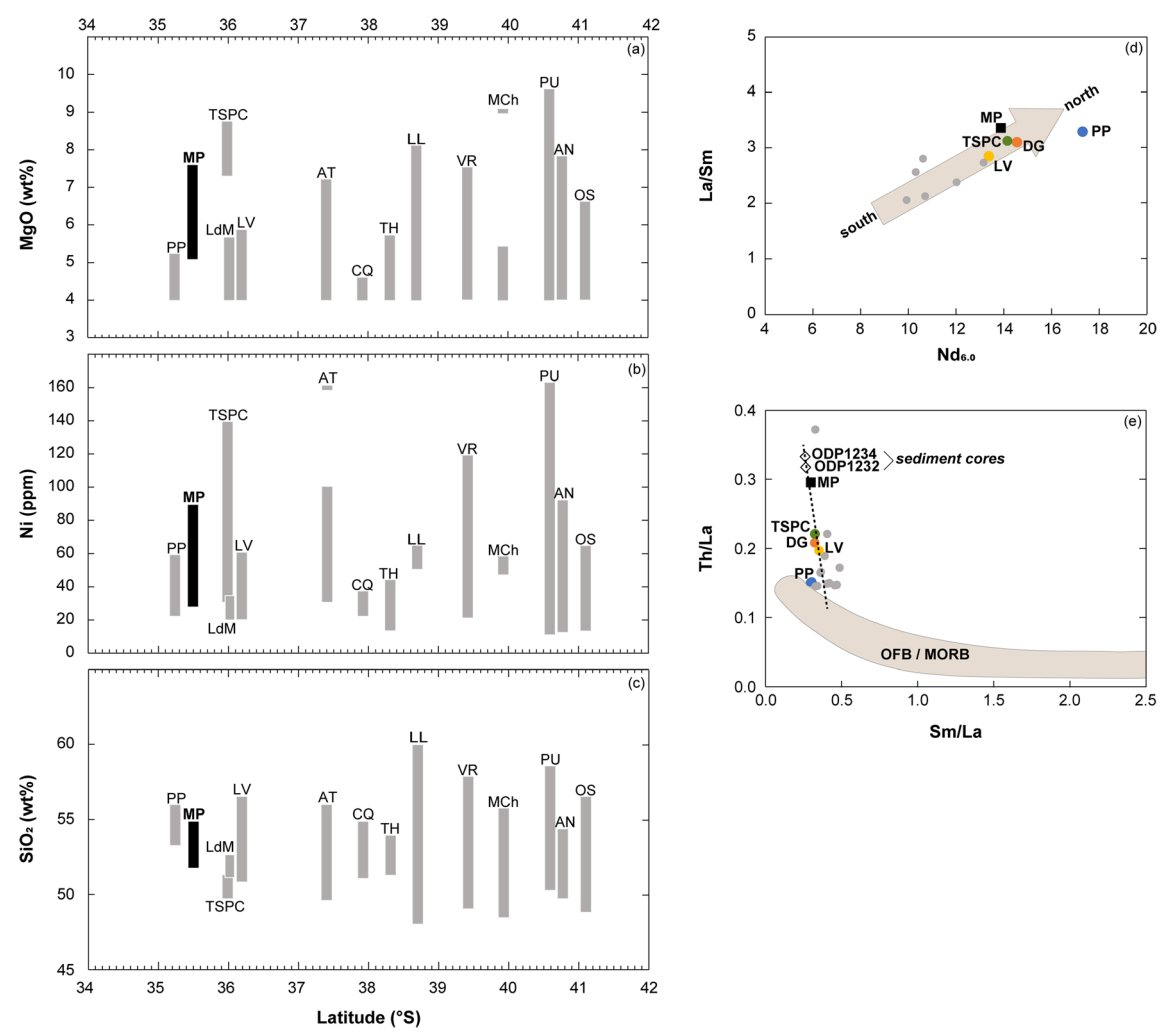


Fig. 10 a-c XRF whole-rock elemental compositions vs latitude provides primitive regional context for how Manantial Pelado compares with nearby systems. Rectangle displays range of data for each specific volcanic center. Data below 4 wt% MgO was removed to focus on the mafic extent of each center, and any data with excessively high MgO was excluded as to not include samples affected by cumulates. Manantial Pelado (this study) and Tatara-San Pedro data only includes mafic samples. All data aside from Manantial Pelado came from a combination of sources including Jacques et al. (2013), Jweda (2014), and Turner et al. (2016), and a compilation of sources from EarthChem (Bouvet De Maisonneuve et al. 2012; Costantini et al. 2011; Deruelle 1982; Gerlach et al. 1988; Hickey-Vargas et al. 1986, 1989, 2002, 2016; Holm et al. 2014; Jacques et al. 2013, 2014; Jicha et al. 2007; Lopez-Escobar et al. 1977, 1981, 1992; López-Escobar et al. 1995; Morgado et al. 2015; Pioli et al. 2015; Rawson et al. 2015; Ruth et al. 2016; Singer et al. 2008; Tormey et al. 1991, 1995; Wehrmann et al. 2014a). Latitudinal order: PP Planchón-Peteroa, MP Manantial Pelado, TSPC Tatara-San Pedro, LdM Laguna del Maule, LV Longavi, AT Antuco, CQ Callaqui, TH

Tolhuaca, LL Llaima, VR Villarrica, MCh Mocho-Choshuenco, PU Puyehue, AN Antillanca, OS Osorno. d, e Incompatible trace element systematics following Turner et al. (2017) to compare Manantial Pelado with PP, DG (Descabezado Grande), TSPC, and LV. Trace element ratios highlight transitional cluster for MP, DG, TSPC, and LV. Colored dots are from Turner et al. (2016) and represent average per volcanic center. Latitudinal order: PP Planchón-Peteroa, MP Manantial Pelado, DG Descabezado Grande, TSPC Tatara-San Pedro, LV Longavi. Gray dots: regional centers from Turner et al. (2016) ranging from 37 to 41° S in latitudinal order: Antuco, Callaqui, Tolhuaca, Llaima, Villarrica, Mocho-Choshuenco, Puyehue, Antillanca, Osorno. e This plot excludes Callaqui, Tolhuaca, and Mocho-Choshuenco due to lack of data for Nd<sub>6,0</sub>. Nd<sub>6,0</sub> for Manantial Pelado data includes averages from 5 to 7 wt% MgO due to data availability. Diamonds: ODP sediment cores offshore Chilean Andes (ODP 1234,  $\sim 36^{\circ}$  S; ODP 1232,  $\sim 40^{\circ}$  S) represent subducting sediments (Plank 2014). Beige polygon: ocean floor basalts (OFB) and mid-ocean ridge basalts (MORB) from Jenner and O'Neill (2012)

fractional crystallization is minimal ( $\sim$ < 10%; potential for olivine accumulation is discussed later). Only the nearby monogenetic cones of Los Hornitos are distinctly more primitive (Figs. 6 and 7); however, they may not be representative of the common mantle melt flux into the crust and long-lived

silicic systems as they bypass zones of storage and homogenization associated with long-lived centers.

We recognize that the basaltic andesites do not represent melt compositions in a strict sense as their textures suggest that significant crystallization occurred. The question is whether the



Bull Volcanol (2020) 82:69 Page 15 of 24 69

crystal cargo remains in suspension, and therefore, whole-rock compositions represent a good approximation to reconstruct melt compositions or whether significant fractionation has taken place. While plagioclase phenocrysts are abundant in the basaltic andesites, the lack of a Eu anomaly and an increase in Sr with increasing SiO<sub>2</sub> in whole-rock compositions suggests that plagioclase fractionation is minimal (Fig. 8, Online Resource B3). This is further corroborated by the fact that core plagioclase compositions are calcic (~An75-89). Moreover, CaO displays a flat trend while Al<sub>2</sub>O<sub>3</sub> and Sc display enriched trends for the basaltic andesite lithology, all of which indicates

no significant pyroxene or spinel fractionation has occurred (Online Resource B3). Thus, only olivine may have been fractionated, which is recognized in the demonstrable continuous depletion in MgO and Ni (Figs. 6 and 7). Following the calculation scheme by Straub et al. (2011) and using the Ni partitioning from Beattie et al. (1991), we calculate olivine fractionation between  $\sim 4$  and 8.5 wt%. This amount of olivine fractionation can account for Ni depletions from a primitive magma of  $\sim 150-250$  ppm (Schmidt and Jagoutz 2017) to 86 ppm as observed in the most primitive basaltic andesites from Manantial Pelado (7.4 wt%; Fig. 7). We therefore argue

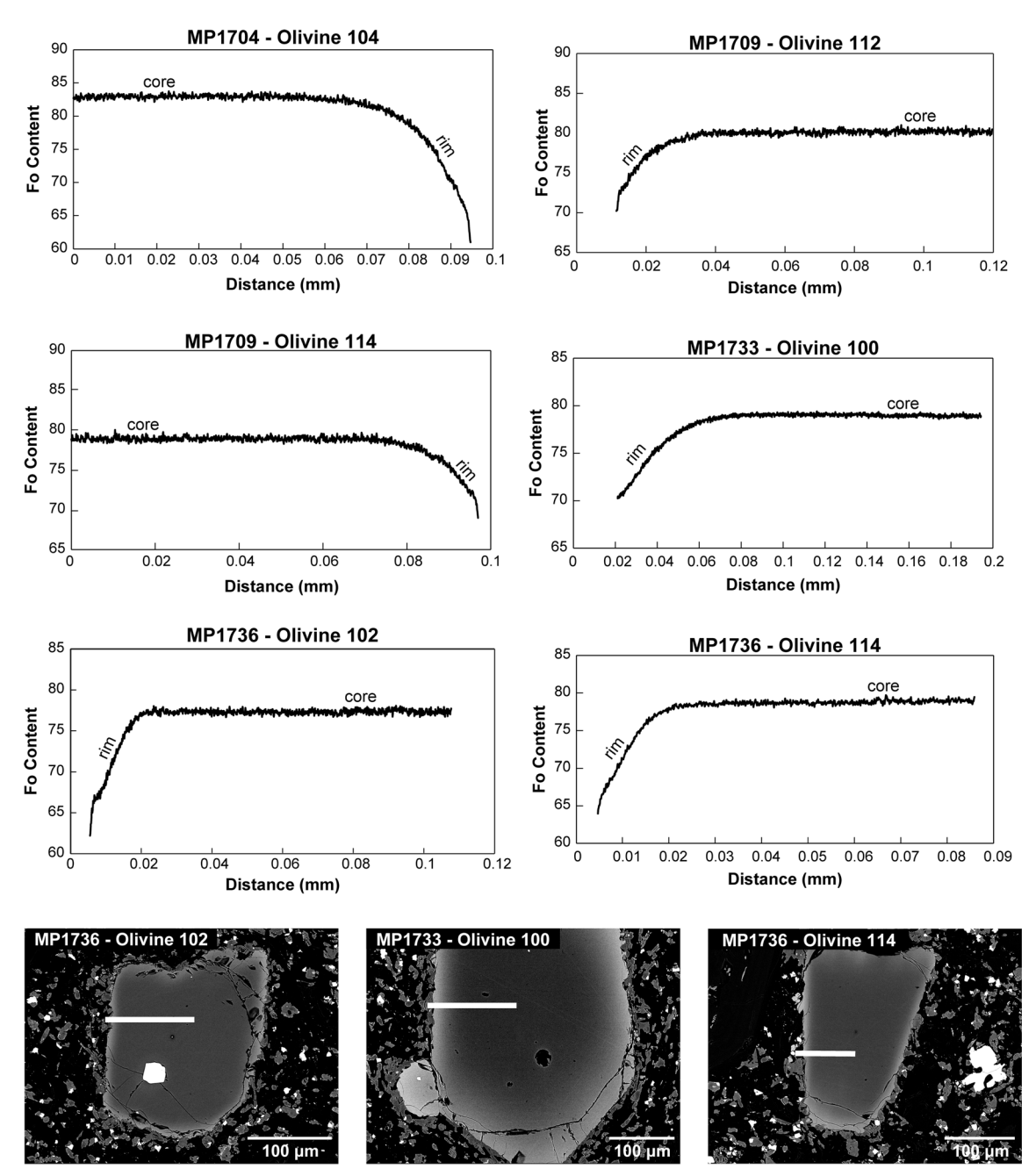


Fig. 11 Olivine transects displaying flat-core characteristics. Transect terminates at end of crystal rim. Back-scattered electron images with respective transect line. Flat cores suggest diffusive re-equilibration. Additional transects and images in Online Resource C1–5

69 Page 16 of 24 Bull Volcanol (2020) 82:69

that magmas from Manantial Pelado experienced minimal amounts of fractionation for most elements and in particular incompatible elements, and that whole-rock data is a close approximation to the primitive mantle-derived melts for this part of the SVZ.

#### Olivine equilibration during long-lived storage

At first sight, this model where Manantial Pelado basaltic andesites are near-primitive compositions with minimal crystal fractionation may be inconsistent with the compositions of the olivine phenocrysts themselves. Fe-Mg partition relationships in olivine would suggest that melts that experienced 4% loss of olivine would still crystallize high Fo (>~Fo<sub>86</sub>) olivines (e.g., Roeder and Emslie 1970; Straub et al. 2011; Ruprecht and Plank 2013) and be not far removed from typical primitive olivine compositions (≥ 90; Sato 1977; Wallace and Carmichael 1999; Kamenetsky et al. 2001; Schmidt and Jagoutz 2017), yet for Manantial Pelado, most olivine cores do not exceed Fo<sub>84</sub> (Figs. 11 and 12). We resolve this conundrum through the fact that these basaltic andesites are likely stored in long-lived processing areas of lower-to-mid crustal conditions where thermal equilibration leads to prolonged presence of partial melts (Dufek and Bergantz 2005; Annen et al. 2006). Temperatures are too cold to retain primitive high-melt fraction magma bodies; instead, crystal-rich mush systems are thought to emerge and persist for a long time. The high crystallinity of Manantial Pelado basaltic andesites is consistent with this model (Fig. 13). It can also explain the much lower Fo content of these olivines. Any normally zoned olivine resulting from crystallization in an evolving melt may equilibrate over time with the reduced melt fraction to lower Fo compositions (Fig. 12), while primitive plagioclase crystals remain zoned due to the slow multi-element diffusion of NaSi-CaAl (Grove et al. 1984).

Manantial Pelado olivine phenocrysts are texturally inconsistent with an unmodified growth process from a primitive liquid. Aside from a few larger glomerocrysts, olivine crystals are subhedral-euhedral grains (~100–200 µm crystal radius) that display relatively flat cores with weak normal zonation limited to the outermost rims of crystals (Figs. 5 and 11). Here we use the term "flat cores" to represent olivine grains that vary internally in major element composition and  $\Delta$ Fo of less than 1 mol%. Furthermore, flat cores comprise > 80% of the crystal radius from the core to the start of the rim zonation. Flat cores either require growth in a melt composition buffered open system (e.g., porous media flow of a large volume of melt passing through a stagnant crystal network; Kelemen et al. 1995) or diffusive equilibration in a thermally buffered system that keeps melt-crystal ratio constant. We disregard porous media flow as it is important for melt transport in the mantle where melts are continuously percolating through solid matrix. In the crust, magma delivery is more episodic (Dufek

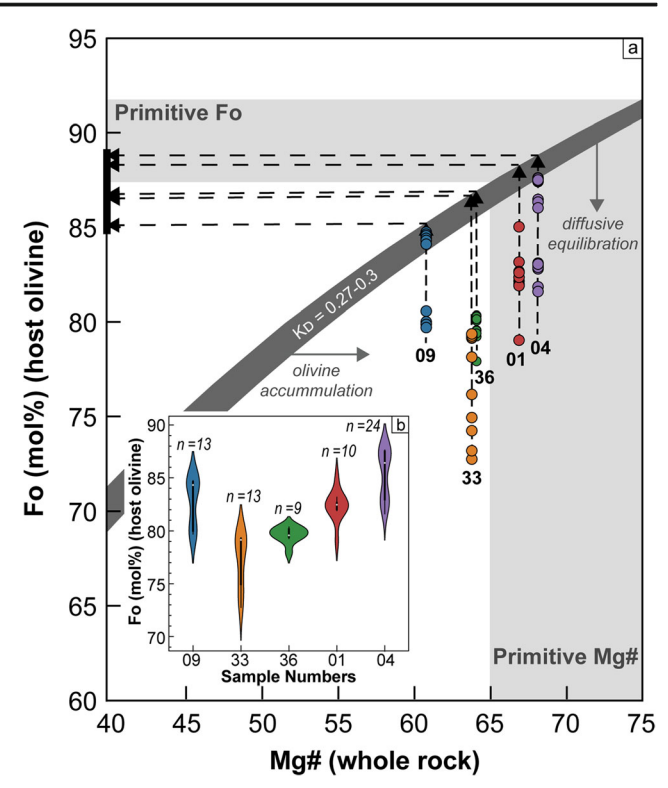


Fig. 12 (a) Fo (host olivine) vs Mg# (whole rock) plotted with the meltliquid equilibrium band ( $K_D = 0.27-0.3$ ) calculated through Mg-Fe partitioning from olivine into the liquid melt (Roeder and Emslie 1970; Toplis 2005). The upper constraint of the melt-liquid equilibrium band is  $K_D = 0.27$ , while the lower constraint is  $K_D = 0.3$ . Mg# calculated on molar basis ((Mg/(Mg + Fe)\*100)) and assumed 20% Fe<sup>3+</sup>. Horizontal deviation from equilibrium line suggests olivine accumulation. Vertical deviation from the equilibrium line is a result of diffusive equilibration. Colored dots: individual olivine core compositions within samples. Numbers: specific MP-17-XX samples. Dashed lines represent samples' path away from equilibrium due to diffusive equilibration and suggests previously elevated Fo (host olivine) in the core. Gray boxes indicating "Primitive Fo" and "Primitive Mg#" are taken from Schmidt and Jagoutz (2017). (b) Inset violin plot: highlights Fo grain density per sample. Sample MP-17-33 displays large range in 12a, and the inset (12b) shows the majority of the grains cluster at higher Fo content (Fo<sub>77-81</sub>)

and Bergantz 2005; Annen et al. 2006). Thus, thermal buffering and diffusive equilibration likely modified those olivines.

While in silicic systems crystal-rich mushes are buffered internally by the eutectic melt composition (Huber et al. 2009), primitive compositions can only be thermally buffered in hot crustal conditions. Those may exist in the lower-to-middle crust where mantle-derived melt emplacement has elevated the geotherm (Dufek and Bergantz 2005; Annen et al. 2006). However, these elevated crustal temperatures may only lead to substantial crustal melting for crust > 50 km (Dufek and Bergantz 2005). For thinner crust, storage and homogenization may dominate.

In temperature-buffered mush systems, initially normally zoned olivines will re-equilibrate to homogenous, unzoned olivines at lower Fo content. Specifically, prolonged residence in a magmatic mush ultimately leads to diffusive equilibration of



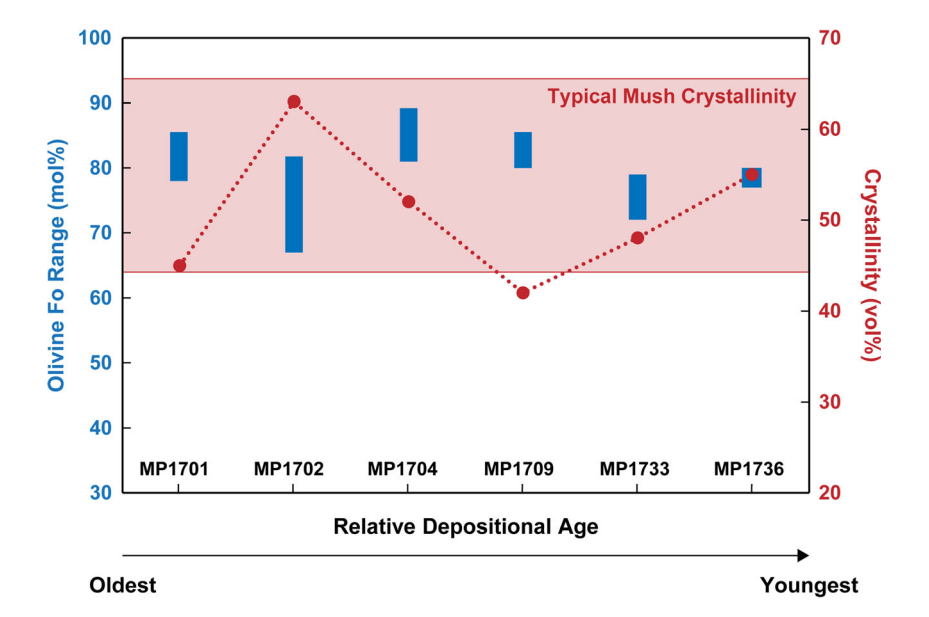
Bull Volcanol (2020) 82:69 Page 17 of 24 69

olivine grains (Costa and Dungan 2005; Oeser et al. 2018). Such diffusion can produce flat-cored olivine that displays lower Fo content in the crystal center compared to the Fo content that originally crystallized. Manantial Pelado lavas contain abundant flat-cored olivine at intermediate Fo content (Figs. 5 and 11). Whether these olivines originate from remobilized cumulates and therefore would be inconsistent with the notion of the Manantial Pelado basaltic andesites representing minimally modified primitive magmas, or whether they document the prolonged equilibration in a primitive mush needs to be answered next.

Manantial Pelado olivines are largely not in equilibrium with liquid compositions represented by the basaltic andesite lavas. Bulk-rock compositions have higher Mg# for the expected Fo relative to equilibrium (Fig. 12;  $K_D^{\text{Ol/liquid}} = 0.27-0.3$ ; Roeder and Emslie 1970; Toplis 2005). Using whole-rock compositions in this plot assumes that the whole rock is a good approximation of the melt in equilibrium with the compared olivines. Although these whole-rock compositions represent approximations of primitive mantle melts, they do not represent the melt in equilibrium with the residing olivine crystals. The current melt composition in equilibrium with the olivine rims, which is the holocrystalline matrix, cannot be measured directly in these lavas. While analyzing the olivine rims or microlites could provide compositional data, it would provide even more depleted compositions in Mg because they reflect the eruptive process and not the late-stage storage. There are two potential explanations for the patterns in Fig. 12. First, commonly, such olivine compositions at low Fo are argued to represent the addition of Mg-rich mineral phases such as olivine (Baggerman and Debari 2011). While such crystal accumulation could explain the horizontal displacement from the equilibrium curve, there is no further textural or chemical evidence of olivine accumulation except for the few glomerocrysts representing a cumulate origin

(Fig. 5). Instead, diffusive equilibration proceeding during crystallization in a mush environment that is thermally and compositionally buffered also shifts olivine compositions to low Fo away from the equilibrium curve linked to whole-rock compositions. As argued before, whole-rock major and trace elements are not showing signs of significant cumulate signatures where additional olivine phenocrysts are being added. Moreover, olivine Ni contents in cumulates with minimal melt present are high at intermediate Fo contents (Oeser et al. 2018) and typically fall significantly to the left of the general Ni-Fo array of olivine phenocrysts. Manantial Pelado olivines are not exceptionally Ni-rich; instead, they tend to be only slightly higher in Ni compared with olivine fractionation, which is consistent with reequilibration of cores and rims at intermediate Ni contents. Thus, for Manantial Pelado lavas, our model considers a compositionally restricted and temperature-buffered system that experiences long-term storage. We suspect there may be a family of primitive magmas that are compositionally very similar making it difficult to distinguish mixing or interaction (Ruprecht and Wörner 2007). This is supported by normal and simple zonation in plagioclase phenocrysts (Fig. 5). The simplistic zoning argues for minimal interaction with diverse compositions and supports long-term storage with similar magmas all prior to rim growth initiated upon ascent. While interaction between similar primitive magmas may be present, we do not see evidence for any felsic interactions, thus determining Manantial Pelado to be a "quasi-closed" system. Therefore, it is open to external heat and mass from similar primitive magmas that all crystallize to  $\sim 55\%$ and experience storage and homogenization, but is closed to highly silicic compositions and interaction such as assimilation and melting of the crust. Potential xenocrysts in Fig. 5 could also represent cores inherited from surrounding crystal-mush domains that have been incorporated and act as a nucleus for

Fig. 13 Olivine Fo and respective crystallinity of Manantial Pelado basaltic andesite samples in order of depositional age. Pervasively high crystallinity (~40–65%) shows Manantial Pelado basaltic andesite display crystal-mush crystallinity. Lack of temporal trend between samples further corroborates the lack of compositional evolution in Manantial Pelado's eruptive products and points towards several crystal-mush reservoirs all from a similar source





69 Page 18 of 24 Bull Volcanol (2020) 82:69

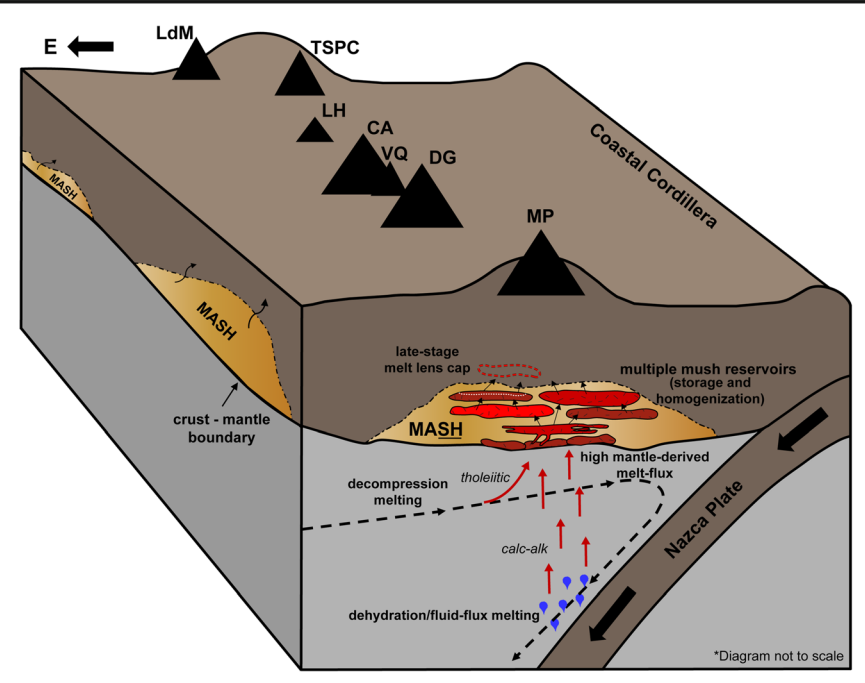


Fig. 14 Manantial Pelado magmatic reservoir schematic. Magmas are stored at mid-to-lower crustal levels and experience homogenization in the hypothesized MASH zone. The magmas are stored in multiple crystal-mush reservoirs of similar compositions where long-term storage and diffusive equilibration can occur. Late-stage crystallization increases after glaciation and results in an evolved, crystal-poor melt lens (white

dashed line). Primarily, homogenized basaltic andesite erupts, but melt lenses of apyhric andesite erupt later in the center's lifetime. The storage in the MASH zone results in homogenized yet still primitive material and high crystallinity in samples suggests storage in crystal-mush reservoirs. MP Manantial Pelado, DG Descabezado Grande, VQ Quizapu, CA Cerro Azul, LH Los Hornitos, TSPC Tatara-San Pedro, LdM Laguna del Maule

further olivine growth. This interpretation would further provide evidence that the system is not fully closed. This compositionally restricted, temperature-buffered, and long-term storage system creates pockets of constant magma composition (Fig. 14). The Fo content of the corresponding olivine decreases as Fe-Mg interdiffusion continuously strives towards equilibrium and produces flat/unzoned homogenous olivine cores. Using the equilibrium curve, we estimate that potential olivine core compositions prior to diffusive equilibration may be as high as ~ Fo<sub>89</sub>, which is consistent with primitive magma compositions (Schmidt and Jagoutz 2017; Fig. 12). While Manantial Pelado olivines re-equilibrate to relatively primitive compositions, they tend to be at the lower extent of the primitive boundary. It is worth noting that re-incorporation of any fractionated olivines (~4-8.5%) has not been taken into account and could elevate original Fo content to higher values within the range of primitive compositions. Ultimately, we argue that Manantial Pelado lavas are not significantly affected by cumulates and instead show batch equilibration in a mush where olivines become flat-cored at lower Fo content than normally would be interpreted to be linked to primitive magma compositions. This also requires that olivine crystallization proceeds significantly so that remaining liquid is significantly depleted in Mg relative to its initial Mg melt content, which is consistent with the high crystallinities in Manantial Pelado lavas (Fig. 13).

While Fe–Mg diffusion can reach the center of an olivine crystal quickly under magmatic conditions, full equilibration takes much longer (Dohmen and Chakraborty 2007). Thus, we need to estimate the amount of time it takes for olivines to fully equilibrate to flat cores. Fe–Mg diffusion is fast with diffusivities D ranging between  $6.4 \times 10^{-18}$  and  $1.1 \times 10^{-16}$  m²/s (Dohmen and Chakraborty 2007) for common parameters required in our model (assuming common magmatic temperatures of basaltic andesites: 1000-1100 °C;  $\Delta NNO + 1$ , 400-700 MPa,  $Fo_{80-90}$ ,  $100-200-\mu m$  crystal radius). We estimate the full equilibration length scale x using a planar-confined source, infinite reservoir relationship of,

$$\Delta c(t) = 0.2 \operatorname{erf}\left(\frac{x}{2\sqrt{Dt}}\right) \tag{1}$$

where the concentration gradient in the core  $\Delta c$  is within 1% of the rim composition (i.e., Fo core < 80.8 for a Fo rim of 80). The factor 0.2 represents the initial variation between core and outer core being 10% and the fact that along that 1D profile elements diffusive from the center to the two opposing crystal rims equally (Fig. 15). Our model relationship will overestimate the time needed to equilibrate the magma as the model is 1D. An initially zoned crystal 200–400  $\mu$ m in diameter with a Fo range of 80–88 from rim to core will equilibrate completely (i.e., to within < 1 mol Fo



Bull Volcanol (2020) 82:69 Page 19 of 24 69

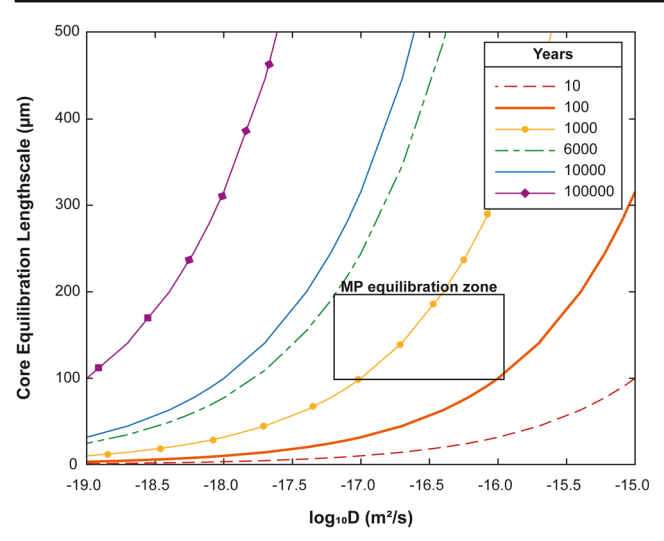


Fig. 15 Equilibration length scale for olivine in mid-to-lower crustal mush conditions. Length scale is estimated assuming an initially zoned olivine crystal with 10% variation in Fo from core to rim and the equilibration timescale following Eq. 1. Length scale x is given for the case where the final concentration in the interior of a crystal of radius x is within 1% of rim concentration. Typical Manantial Pelado flat-cored olivine (100–200- $\mu$ m radius) stored in a mafic crustal mush system would equilibrate as fast as 100 years. Average equilibration timescales are likely on the order of a few 1000 years. Black rectangle: equilibration zone for Manantial Pelado olivine

unit) in 25 to 6000 years. This suggests that any normal zoning developed during magma crystallization can be erased in a mafic mush in a timeframe where magma and mush conditions do not change much and temperatures remain high. It also suggests that flat-cored olivines are not necessary to reflect cumulate involvement but can represent batch equilibration of a quasi-closed system.

In summary, whole-rock concentrations of Manantial Pelado basaltic andesites represent near-primitive compositions with a minimal differentiation history in the crust (Figs. 6, 7, and 10). In fact, Manantial Pelado samples are among the most primitive magmas in the SVZ with Mg# ranging between 61 and 68. These lavas are representative of melts that are still in equilibrium with typical mantle lithologies (Schmidt and Jagoutz 2017). Importantly, olivine major element compositions can be misleadingly interpreted to represent evolved magmas. Diffusive equilibration within olivine suggests these phenocrysts were once near Fo<sub>90</sub>. Considered together with the presence of Cr-spinel inclusions in olivine cores, these observations suggest that the crystal record is consistent with the primitive nature of Manantial Pelado lavas (Fig. 5).

#### Lithologic relationships

Expanding the discussion to the other lithologies, trace element systematics suggest that the evolved andesite compositions are mainly a result of fractionation from the near-primitive basaltic andesite. Crystal-rich mushes typically reach rheologic lock up at crystal contents > 60% (Marsh 1988). The reduced mobility may facilitate the extraction of a more evolved melt lens cap (Dufek and Bachmann 2010). Such a melt lens may be represented by the aphyric andesites. Thus, while Manantial Pelado predominantly generated homogenous basaltic andesite, as a 45–55% crystalline mush is still eruptible, its late-stage activity may have had an increase in crystallization and slowed convection. This change in behavior could allow for the formation of an evolved, crystal-poor, melt lens which resulted in the eruption of the aphyric andesite.

The ages of the near-primitive basaltic andesite compared with the evolved aphyric andesite reveal that although they may be genetically related, they occur during different time periods of Manantial Pelado's history. Basaltic andesite predominantly erupted only from ~220 to 190 ka, while the aphyric andesite are much younger (~30 ka; Table 1). We suspect these two lithologies are genetically related (Fig. 8) but are temporally very distinct. One can assume Manantial Pelado erupted predominantly basaltic andesite, experienced a period of dormancy, and then erupted a new lithology from the same original source. A potential cause for this dormancy coincides with glaciation (Rabassa and Clapperton 1990), which is consistent with glacial striations found on top of basaltic andesites. Following that dormancy, we see that Manantial Pelado went from erupting porphyritic basaltic andesite into erupting the efficiently differentiated melt lens of the basaltic andesite mush to create the aphyric andesite within ~170 ka (Table 1).

#### **Crustal magma assembly**

In an area surrounded by active silicic volcanism, further characterization of primitive magmas that could contribute to the upper crustal systems is crucial in understanding eruption dynamics and temporal evolution of volcanic systems. Placing our results into the context of a SVZ MASH model (Hildreth and Moorbath 1988), we suggest that magma generation at Manantial Pelado may have encountered a high mantlederived melt flux MASH zone in the mid-to-lower crust (Fig. 14). Its primitive nature was retained in a quasi-closed system where mainly storage and homogenization processes were at play, and effects of melting and assimilation are subordinate (Fig. 14). Manantial Pelado produces a significant amount of homogenous material throughout its history, and the main lithologies are near-primitive and do not display mixing trends with evolved crustal-derived melts. Phenocrysts do not prove to be foreign, but to fully determine their provenance isotope data is necessary but beyond the scope of this study. MASH zones may be more complex and require further investigation to explain how primitive magmas reach the surface without significant crustal contribution as evidenced by small-volume eruptions at nearby monogenetic cinder cones



69 Page 20 of 24 Bull Volcanol (2020) 82:69

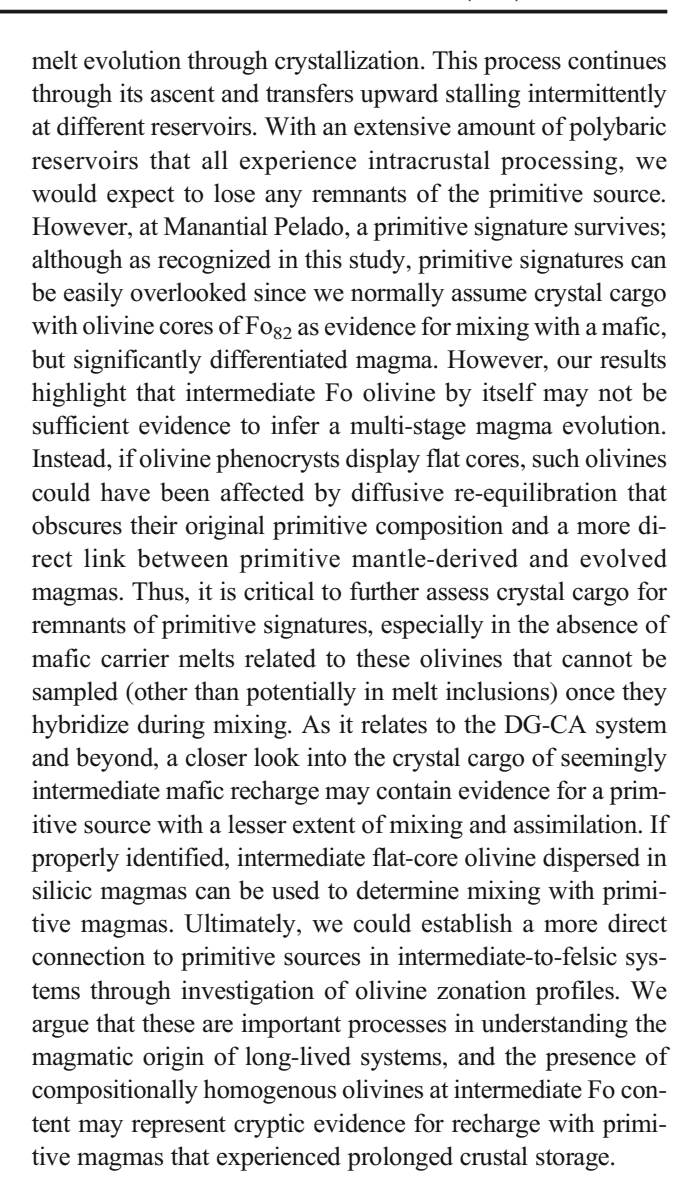
(Salas et al. 2017). We envision that the MASH zone may be compositionally compartmentalized depending on the frequency and accumulation of added mantle melt (Dufek and Bergantz 2005). As a result, some regions in the lower-to-middle crust experience high input of mantle-derived magma that shields mush lenses from significant crustal contributions (Fig. 14). MASH zones have not been imaged in great spatial detail limiting our ability to identify their internal structure and recognizing potential pathways for more mantle-like magmas.

The high crystallinity and narrow compositional range of these lavas point towards processes that reduce compositional diversity while not fully erasing it. We envision a crystalmush storage system for these basaltic andesites (Bachmann and Bergantz 2004; Hildreth 2004; Schleicher and Bergantz 2017). Manantial Pelado displays crystal-mush storage textures and compositions with its high crystallinity, mafic composition, and rare glomerocryst textures (Figs. 5, 12, and 13). While there are minor compositional variations between the lavas, the overall lack of zonation or evolution between flows (Fig. 13) suggests the storage region never developed and extracted more evolved magmas potentially due to frequent disruption of individual mush lenses. The lack of a temporal trend between samples further corroborates the lack of compositional evolution in Manantial Pelado's eruptive products and points towards several crystal-mush reservoirs all from a similar source (Figs. 13 and 14). We refer to them as quasiclosed system, because they developed only small compositional diversity. This explains the presence of flat cores in the olivine as prolonged storage that not only just promoted olivine growth but also re-equilibrated to flat-cored olivines. The overall homogenous nature of the lavas with slight compositional and textural variation could be explained by multiple crystal-mush storage systems within the crust that all originated from the same mantle source (Figs. 13 and 14).

#### Insight for nearby silicic systems

This study has established that evaluating the primitive extent of a system requires an analysis of the bulk composition, the mineralogy and their composition, and the potential overprinting of the latter during prolonged storage. The presence of compositionally slightly evolved olivines does not imply that the bulk magma is evolved and has a complex assembly history. Instead, diffusive re-equilibration in a primitive bulk system may mask a protracted history that results in lower Mg flat-cored olivines.

Recent studies have considered magmatic storage to be transcrustal or polybaric (Hildreth and Moorbath 1988; Cashman et al. 2017), where an initially primitive and mantle-sourced magma is injected into the lower crust that continually feeds successive overlaying reservoirs distributed through the upper crust. These consecutive reservoirs experience partial melting of surrounding crust and compositional



#### **Conclusion**

A variety of methods and calculations were used to characterize the primitive nature and storage processes of Manantial Pelado. Whole-rock compositions paired with mineral-scale data provide reservoir constraints and insight into magma chamber processes. Manantial Pelado's dominant lithology, basaltic andesite, yielded a weighted mean age of  $209 \pm 6.3$  ka ( $2\sigma$ ; MSWD = 1.16) and all of these lavas erupted over a short time interval < 20 kyr. Additionally, the basaltic andesite lavas display near-primitive compositions through presence of Cr-spinels, elevated Mg#, and Ni content. Manantial Pelado lavas plot at the lower boundary for global primitive arcs and are among the most primitive magmas in regional volcanic centers excluding cinder cones. By constraining the amount of fractionation and equilibration of the system as well as noting the textural evidence of flat cores, Manantial Pelado



Bull Volcanol (2020) 82:69 Page 21 of 24 69

proved to be more primitive than initial results suggested due to diffusive equilibration. Prior to diffusive equilibration, olivine phenocrysts may have contained up to Fo<sub>91</sub> cores. After modeling the timescales of diffusion, we suggest this equilibration occurred on the order of several thousand years. Manantial Pelado fits into some aspects of the MASH model by experiencing storage and homogenization in the lower crust sourced from high mantle-derived melt flux and is followed by long-term residence in multiple crystal-mush reservoirs. We suggest that in our system, the MASH zone is not effective in providing much melting or assimilation, which could be related to Manantial Pelado residing in the transitional segment of the SVZ. Manantial Pelado is located at the boundary between geochemical arc variations caused by effective MASH processes (> 50 km) or variations caused by mantle heterogeneities in thinner crust. Instead, we envision Manantial Pelado (at a transitional boundary) to experience the storage and homogenization aspects of MASH that occur in pockets within lower crustal storage regions and become sufficiently isolated from significant crustal input.

There remains a substantial need to characterize and study long-lived primitive stratocones in the SVZ to reveal the interplay of crustal processes of storage and magma evolution with changes in magma input from the mantle. With the use of textural, whole-rock data, mineral data, and geochronology, we were able to provide insight into one of the few mafic exposures within the SVZ. Manantial Pelado encountered long-term storage and proves to be a primitive stratocone exposed at the surface of thickened crust.

Acknowledgments Field work was greatly assisted by Pablo Salas and Paulina Henry. Thanks go to Paul Carpenter (WUSTL) and Frank Tepley (OSU) for electron microprobe assistance and advice. We greatly appreciate the discussions and support provided by Max Gavrilenko and Ellyn Huggins. We thank Nicole Métrich and Andrew Harris for the excellent editorial handling as well as two anonymous reviewers. Additionally, we would like to thank USGS internal reviewers Dawn Ruth and Michael Clynne for their constructive comments and reviews of this paper.

**Funding** This study was funded by the US National Science Foundation (EAR-1719687 and 1717288 to PR).

#### **Compliance with ethical standards**

**Disclaimer** Any use of trade, firm, or product names is for descriptive purposes only, and does not imply endorsement by the United States government.

#### References

Andersen NL, Singer BS, Jicha BR, Beard BL, Johnson CM, Licciardi JM (2017) Pleistocene to Holocene growth of a large upper crustal rhyolitic magma reservoir beneath the active Laguna del Maule volcanic field, Central Chile. J Petrol 58:85–114

- Annen C, Blundy JD, Sparks RSJ (2006) The genesis of intermediate and silicic magmas in deep crustal hot zones. J Petrol 47:505–539
- Bachmann O, Bergantz GW (2003) Rejuvenation of the Fish Canyon magma body: a window into the evolution of large-volume silicic magma systems. Geology 31:789–792
- Bachmann O, Bergantz GW (2004) On the origin of crystal-poor rhyolites: extracted from batholithic crystal mushes. J Petrol 45:1565–1582
- Baggerman TD, DeBari SM (2011) The generation of a diverse suite of Late Pleistocene and Holocene basalt through dacite lavas from the northern Cascade arc at Mount Baker, Washington. Contrib Mineral Petrol 161(1):75–99
- Beattie P, Ford C, Russell D (1991) Partition coefficients for olivine-melt and orthopyroxene-melt systems. Contrib Mineral Petrol 109(2): 212–224
- Bouvet De Maisonneuve C, Dungan MA, Bachmann O, Burgisser A (2012) Insights into shallow magma storage and crystallization at Volcán Llaima (Andean southern volcanic zone, Chile). J Volcanol Geotherm Res 211:76–91
- Burns DH, de Silva SL, Tepley FJ, Schmitt AK (2019) Chasing the mantle: deciphering cryptic mantle signals through Earth's thickest continental magmatic arc. Earth Planet Sci Lett 531:115985
- Calvert AT, Lanphere MA (2006) Argon geochronology of Kilauea's early submarine history. J Volcanol Geotherm Res 151:1–18. https://doi.org/10.1016/j.jvolgeores.2005.07.023
- Cashman KV, Sparks RSJ, Blundy JD (2017) Vertically extensive and unstable magmatic systems: a unified view of igneous processes. Science 355(6331):eaag3055
- Cembrano J, Lara L (2009) The link between volcanism and tectonics in the southern volcanic zone of the Chilean Andes: a review. Tectonophysics 471(1–2):96–113
- Clynne MA, Borg LE (1997) Olivine and chromian spinel in primitive calc-alkaline and tholeiitic lavas from the southernmost Cascade Range, California; a reflection of relative fertility of the source. Can Mineral 35(2):453–472
- Conrad WK, Kay RW (1984) Ultramafic and mafic inclusions from Adak Island: crystallization history, and implications for the nature of primary magmas and crustal evolution in the Aleutian Arc. J Petrol 25(1):88–125
- Conrey RM, Hooper PR, Larson PB, Chesley J, Ruiz J (2001) Trace element and isotopic evidence for two types of crustal melting beneath a High Cascade volcanic center, Mt. Jefferson, Oregon. Contrib Mineral Petrol 141(6):710–732
- Costa F, Dungan MA (2005) Short time scales of magmatic assimilation from diffusion modeling of multiple elements in olivine. Geology 33:837–840
- Costantini L, Pioli L, Bonadonna C, Clavero J, Longchamp C (2011) A late Holocene explosive mafic eruption of Villarrica volcano, Southern Andes: the Chaimilla deposit. J Volcanol Geotherm Res 200(3–4):143–158. https://doi.org/10.1016/j.jvolgeores.2011.09.010
- Dalrymple GB, Alexander EC, Lanphere MA, Kraker GP (1981) Irradiation of samples for <sup>40</sup>Ar/<sup>39</sup>Ar dating using the Geological Survey TRIGA reactor. U S Geol Surv Prof Pap 1176:55. https://doi.org/10.3133/pp1176
- Deruelle B (1982) Petrology of the Plio-Quaternary volcanism of the south-central and meridional Andes. J Volcanol Geotherm Res 14(1–2):77–124. https://doi.org/10.1016/0377-0273(82)90044-0
- Dohmen R, Chakraborty S (2007) Fe–Mg diffusion in olivine II: point defect chemistry, change of diffusion mechanisms and a model for calculation of diffusion coefficients in natural olivine. Phys Chem Miner 34:409–430
- Drake MJ, Weill DF (1975) Partition of Sr, Ba, Ca, Y, Eu2+, Eu3+, and other REE between plagioclase feldspar and magmatic liquid: an experimental study. Geochim Cosmochim Acta 39(5):689–712



69 Page 22 of 24 Bull Volcanol (2020) 82:69

- Dufek J, Bachmann O (2010) Quantum magmatism: magmatic compositional gaps generated by melt-crystal dynamics. Geology 38:687–690
- Dufek J, Bergantz GW (2005) Lower crustal magma genesis and preservation: a stochastic framework for the evaluation of basalt–crust interaction. J Petrol 46:2167–2195
- Dungan MA, Wulff A, Thompson REN (2001) Eruptive stratigraphy of the Tatara–San Pedro complex, 36 S, Southern Volcanic Zone, Chilean Andes: reconstruction method and implications for magma evolution at long-lived arc volcanic centers. J Petrol 42:555–626
- Fleck R, Sutter J, Elliot D (1977) Interpretation of discordant 40Ar/39Ar agespectra of Mesozoic tholeiites from Antarctica. Geochim Cosmochim Acta 41:15–32
- Fleck RJ, Hagstrum JT, Calvert AT (2014) <sup>40</sup>Ar/<sup>39</sup>Ar geochronology, paleomagnetism, and evolution of the Boring volcanic field, Oregon and Washington, USA. Geosphere 10:1283–1314. https://doi.org/10.1130/GES00985.1
- Fleck RJ, Calvert AT, Coble MA (2019) Characterization of the rhyolite of Bodie Hills and <sup>40</sup>Ar/<sup>39</sup>Ar intercalibration with Ar mineral standards. Chem Geol 525:282–302. https://doi.org/10.1016/j.chemgeo. 2019.07.022
- Fontijn K, Lachowycz SM, Rawson H, Pyle DM, Mather TA, Naranjo JA, Moreno-Roa H (2014) Late Quaternary tephrostratigraphy of southern Chile and Argentina. Quat Sci Rev 89:70–84
- Gavrilenko M, Ozerov A, Kyle PR, Carr MJ, Nikulin A, Vidito C, Danyushevsky L (2016) Abrupt transition from fractional crystallization to magma mixing at Gorely volcano (Kamchatka) after caldera collapse. Bull Volcanol 78(7):47
- Gerlach DC, Frey FA, Moreno-Roa H, Lopez-Escobar L (1988) Recent volcanism in the Puyehue—Cordon Caulle region, Southern Andes, Chile (40· 5° S): petrogenesis of evolved lavas. J Petrol 29(2):333–382. https://doi.org/10.1093/petrology/29.2.333
- Grove TL, Baker MB, Kinzler RJ (1984) Coupled CaAl-NaSi diffusion in plagioclase feldspar: experiments and applications to cooling rate speedometry. Geochim Cosmochim Acta 48:2113–2121
- Grunder AL (1987) Low  $\delta$ 18O silicic volcanic rocks at the Calabozos caldera complex, southern Andes. Contrib Mineral Petrol 95:71–81
- Hawkesworth CJ, Hammill M, Gledhill AR, van Calsteren P, Rogers G (1982) Isotope and trace element evidence for late-stage intra-crustal melting in the High Andes. Earth Planet Sci Lett 58(2):240–254
- Hickey-Vargas R, Frey FA, Gerlach DC, López-Escobar L (1986) Multiple sources for basaltic arc rocks from the southern volcanic zone of the Andes (34-41 S): trace element and isotopic evidence for contributions from subducted oceanic crust, mantle and continental crust. J Geophys Res-Solid Earth 91(6):5963–5983. https://doi.org/ 10.1029/JB091iB06p05963
- Hickey-Vargas R, Moreno-Roa H, López-Escobar L, Frey FA (1989) Geochemical variations in Andean basaltic and silicic lavas from the Villarrica-Lanin volcanic chain (39.5 S): an evaluation of source heterogeneity, fractional crystallization and crustal assimilation. Contrib Mineral Petrol 103(3):361–386. https://doi.org/10.1007/ BF00402922
- Hickey-Vargas R, Sun M, López-Escobar L, Moreno-Roa H, Reagan MK, Morris JD, Ryan JG (2002) Multiple subduction components in the mantle wedge: evidence from eruptive centers in the Central Southern volcanic zone, Chile. Geology 30(3):199–202. https://doi.org/10.1130/0091-7613(2002)030<0199:MSCITM>2.0.CO;2
- Hickey-Vargas R, Holbik S, Tormey D, Frey FA, Roa HM (2016)
  Basaltic rocks from the Andean Southern Volcanic Zone: insights from the comparison of along-strike and small-scale geochemical variations and their sources. Lithos 258:115–132. https://doi.org/10.1016/j.lithos.2016.04.014
- Hildreth W (2004) Volcanological perspectives on Long Valley, Mammoth Mountain, and Mono Craters: several contiguous but discrete systems. J Volcanol Geotherm Res 136:169–198

- Hildreth W, Drake RE (1992) Volcán Quizapú, Chilean Andes. Bull Volcanol 54:93–125
- Hildreth W, Moorbath S (1988) Crustal contributions to arc magmatism in the Andes of central Chile. Contrib Mineral Petrol 98:455–489
- Hildreth W, Godoy E, Fierstein J, Singer B (2010) Laguna del Maule Volcanic field: eruptive history of a Quaternary basalt-to-rhyolite distributed volcanic field on the Andean range crest in central Chile. Servicio Nacional de Geología y Minería-Chile Boletin 63: 142
- Hildreth W, Grunder AL, Drake RE (1984) The Loma Seca Tuff and the Calabozos caldera: a major ash-flow and caldera complex in the southern Andes of central Chile. Geol Soc Am Bull 95:45–54
- Holm PM, Søager N, Dyhr CT, Nielsen MR (2014) Enrichments of the mantle sources beneath the Southern Volcanic Zone (Andes) by fluids and melts derived from abraded upper continental crust. Contrib MineralPetrol 167(5):1004. https://doi.org/10.1007/ s00410-014-1004-8
- Huber C, Bachmann O, Manga M (2009) Homogenization processes in silicic magma chambers by stirring and mushification (latent heat buffering). Earth Planet Sci Lett 283(1–4):38–47
- Jacques G, Hoernle K, Gill J, Hauff F, Wehrmann H, Garbe-Schönberg D, van den Bogaard P, Bindeman I, Lara LE (2013) Across-arc geochemical variations in the Southern Volcanic Zone, Chile (34.5–38.0 S): constraints on mantle wedge and slab input compositions. Geochim Cosmochim Acta 123:218–243
- Jacques G, Hoernle K, Gill J, Wehrmann H, Bindeman I, Lara LE (2014) Geochemical variations in the Central Southern Volcanic Zone, Chile (38–43 S): the role of fluids in generating arc magmas. Chem Geol 371:27–45
- James DE (1982) A combined O, Sr, Nd, and Pb isotopic and trace element study of crustal contamination in central Andean lavas, I. Local geochemical variations. Earth Planet Sci Lett 57(1):47–62
- Jenner FE, O'Neill HSC (2012) Analysis of 60 elements in 616 ocean floor basaltic glasses. Geochem Geophys Geosyst 13(2)
- Jicha BR, Singer BS, Beard BL, Johnson CM, Moreno-Roa H, Naranjo JA (2007) Rapid magma ascent and generation of 230Th excesses in the lower crust at Puyehue–Cordón Caulle, Southern Volcanic Zone, Chile. Earth Planet Sci Lett 255(1–2):229–242. https://doi.org/10.1016/j.epsl.2006.12.017
- Johnson D, Hooper P, Conrey R (1999) XRF method XRF analysis of rocks and minerals for major and trace elements on a single low dilution Li-tetraborate fused bead. Adv X-ray Anal 41:843–867
- Jweda J (2014) Geochemistry of the Tatara-San Pedro continental arc volcanic complex and implications for magmatism in the Chilean Southern Volcanic Zone. Ph.D. Dissertation Columbia University 316pp
- Kamenetsky VS, Crawford AJ, Meffre S (2001) Factors controlling chemistry of magmatic spinel: an empirical study of associated olivine, Cr-spinel and melt inclusions from primitive rocks. J Petrol 42:655–671
- Kelemen PB, Whitehead JA, Aharonov E, Jordahl KA (1995) Experiments on flow focusing in soluble porous media, with applications to melt extraction from the mantle. J Geophys Res-Solid Earth 100:475–496
- Le Maitre RW, Streckeisen A, Zanettin B, Le Bas MJ, Bonin P, Bateman P, Bellini G, Dudek A, Efremova S, Keller J, Lameyre J (2002) Igneous rocks: a classification of and glossary of terms. Recommendations of the International Union of Geological Sciences (IUGS), Subcommission on the Systematics of Igneous Rocks
- Lee JY, Marti K, Severinghaus JP (2006) A redetermination of the isotopic abundances of atmospheric Ar. Geochim Cosmochim Acta 70: 4507–4512. https://doi.org/10.1016/j.gca.2006.06.1563
- Lopez-Escobar L, Frey FA, Vergara M (1977) Andesites and highalumina basalts from the central-south Chile High Andes:



Bull Volcanol (2020) 82:69 Page 23 of 24 69

- geochemical evidence bearing on their petrogenesis. Contrib Mineral Petrol 63(3):199–228. https://doi.org/10.1007/BF00375573
- Lopez-Escobar L, Vergara M, Frey FA (1981) Petrology and geochemistry of lavas from Antuco volcano, a basaltic volcano of the Southern Andes (37° 25' S). J Volcanol Geotherm Res 11(2–4): 329–352. https://doi.org/10.1016/0377-0273(81)90030-5
- Lopez-Escobar L, Parada MA, Moreno H, Frey FA, Hickey-Vargas RL (1992) A contribution to the petrogenesis of Osomo and Calbuco volcanoes, Southern Andes (41° 00′-41° 30′S): comparative study. Andean Geol 19(2):211–226
- López-Escobar L, Cembrano J, Moreno H (1995) Geochemistry and tectonics of the Chilean Southern Andes basaltic Quaternary volcanism (37-46S). Andean Geol 22:219–234. https://doi.org/10.5027/ andgeoV22n2-a06
- Marsh BD (1988) Crystal capture, sorting, and retention in convecting magma. Geol Soc Am Bull 100:1720–1737
- McDonough WF, Sun SS (1995) The composition of the earth. Chem Geol 120(3–4):223–253
- Morgado E, Parada MA, Contreras C, Castruccio A, Gutiérrez F, McGee LE (2015) Contrasting records from mantle to surface of Holocene lavas of two nearby arc volcanic complexes: Caburgua-Huelemolle Small Eruptive Centers and Villarrica Volcano, Southern Chile. J Volcanol Geotherm Res 306:1–16. https://doi.org/10.1016/j.jvolgeores.2015.09.023
- Oeser M, Ruprecht P, Weyer S (2018) Combined Fe-Mg chemical and isotopic zoning in olivine constraining magma mixing-to-eruption timescales for the continental arc volcano Irazú (Costa Rica) and Cr diffusion in olivine. Am Mineral 103:582–599
- Pioli L, Scalisi L, Costantini L, Di Muro A, Bonadonna C, Clavero J (2015) Explosive style, magma degassing and evolution in the Chaimilla eruption, Villarrica volcano, Southern Andes. Bull Volcanol 77(11):93
- Plank T (2005) Constraints from thorium/lanthanum on sediment recycling at subduction zones and the evolution of the continents. J Petrol 46(5):921–944
- Plank T (2014) The chemical composition of subducting sediments.
- Rabassa J, Clapperton CM (1990) Quaternary glaciations of the southern Andes. Quat Sci Rev 9:153–174
- Ramos VA, Cegarra M, Cristallini E (1996) Cenozoic tectonics of the High Andes of west-central Argentina (30–36 S latitude). Tectonophysics 259:185–200
- Rawson H, Naranjo JA, Smith VC, Fontijn K, Pyle DM, Mather TA, Moreno H (2015) The frequency and magnitude of post-glacial explosive eruptions at Volcán Mocho-Choshuenco, southern Chile. J Volcanol Geotherm Res 299:103–129. https://doi.org/10.1016/j. jvolgeores.2015.04.003
- Renne PR, Swisher CC, Deino AL, Karner DB, Owens TL, DePaolo DJ (1998) Intercalibration of standards, absolute ages and uncertainties in 40Ar/39Ar dating. Chem Geol 145:117–152
- Rodríguez C, Sellés D, Dungan M, Langmuir C, Leeman W (2007) Adakitic dacites formed by intracrustal crystal fractionation of water-rich parent magmas at Nevado de Longaví volcano (36.2S; Andean Southern Volcanic Zone, Central Chile). J Petrol 48:2033– 2061
- Roeder PL, Emslie R (1970) Olivine-liquid equilibrium. Contrib Mineral Petrol 29:275–289
- Ruprecht P, Bachmann O (2010) Pre-eruptive reheating during magma mixing at Quizapú volcano and the implications for the explosiveness of silicic arc volcanoes. Geology 38:919–922
- Ruprecht P, Plank T (2013) Feeding andesitic eruptions with a high-speed connection from the mantle. Nature 500:68–72
- Ruprecht P, Wörner G (2007) Variable regimes in magma systems documented in plagioclase zoning patterns: El Misti stratovolcano and Andahua monogenetic cones. J Volcanol Geotherm Res 165:142–162. https://doi.org/10.1016/j.jvolgeores.2007.06.002

- Ruprecht P, Bergantz GW, Cooper KM, Hildreth W (2012) The crustal magma storage system of Volcán Quizapú, Chile, and the effects of magma mixing on magma diversity. J Petrol 53:801–840
- Ruth DC, Cottrell E, Cortés JA, Kelley KA, Calder ES (2016) From passive degassing to violent Strombolian eruption: the case of the 2008 eruption of Llaima volcano, Chile. J Petrol 57(9):1833–1864. https://doi.org/10.1093/petrology/egw063
- Salas PA, Rabbia OM, Hernández LB, Ruprecht P (2017) Mafic monogenetic vents at the Descabezado Grande volcanic field (35.5°S–70.8°W): the northernmost evidence of regional primitive volcanism in the Southern Volcanic Zone of Chile. Int J Earth Sci 106:1107–1121
- Sato H (1977) Nickel content of basaltic magmas: identification of primary magmas and a measure of the degree of olivine fractionation. Lithos 10:113–120
- Schleicher JM, Bergantz GW (2017) The mechanics and temporal evolution of an open-system magmatic intrusion into a crystal-rich magma. J Petrol 58:1059–1072. https://doi.org/10.1093/petrology/egx045
- Schmidt MW, Jagoutz O (2017) The global systematics of primitive arc melts. Geochem Geophys Geosyst 18:2817–2854
- Sellés D, Rodríguez A, Dungan MA, Naranjo JA, Gardeweg M (2004) Geochemistry of Nevado de Longaví Volcano (36.2 S): a compositionally atypical arc volcano in the Southern Volcanic Zone of the Andes. Rev Geol Chile 31(2):293–315
- Singer BS, Jicha BR, Harper MA, Naranjo JA, Lara LE, Moreno-Roa H (2008) Eruptive history, geochronology, and magmatic evolution of the Puyehue-Cordón Caulle volcanic complex, Chile. Geol Soc Am Bull 120(5–6):599–618. https://doi.org/10.1130/B26276.1
- Steiger RH, Jäger E (1977) Subcommission on geochronology: convention on the use of decay constants in geo- and cosmochronology. Earth Planet Sci Lett 36:359–362. https://doi.org/10.1016/0012-821X(77)90060-7
- Stern CR (2004) Active Andean volcanism: its geologic and tectonic setting. Rev Geol Chile 3:161–206
- Stern CR, Kilian R (1996) Role of the subducted slab, mantle wedge and continental crust in the generation of adakites from the Andean Austral Volcanic Zone. Contrib Mineral Petrol 123:263–281
- Straub SM, Gomez-Tuena A, Stuart FM, Zellmer GF, Espinasa-Perena R, Cai Y, Iizuka Y (2011) Formation of hybrid arc andesites beneath thick continental crust. Earth Planet Sci Lett 303:337–347
- Tassara A, Echaurren A (2012) Anatomy of the Andean subduction zone: three-dimensional density model upgraded and compared against global-scale models. Geophys J Int 189:161–168
- Toplis MJ (2005) The thermodynamics of iron and magnesium partitioning between olivine and liquid: criteria for assessing and predicting equilibrium in natural and experimental systems. Contrib Mineral Petrol 149(1):22–39
- Tormey DR, Hickey-Vargas R, Frey FA, López-Escobar L (1991) Recent lavas from the Andean volcanic front (33 to 42 S); interpretations of along-arc compositional variations. Geol Soc Am Spec Pap 265:57–77. https://doi.org/10.1130/SPE265-p57
- Tormey DR, Frey FA, Lopez-Escobar L (1995) Geochemistry of the active Azufre-Planchon-Peteroa volcanic complex, Chile (35 15' S): evidence for multiple sources and processes in a cordilleran arc magmatic system. J Petrol 36(2):265–298. https://doi.org/10.1093/ petrology/36.2.265
- Turner SJ, Langmuir CH, Katz RF, Dungan MA, Escrig S (2016)
  Parental arc magma compositions dominantly controlled by
  mantle-wedge thermal structure. Nat Geosci 9:772–776
- Turner SJ, Langmuir CH, Dungan MA, Escrig S (2017) The importance of mantle wedge heterogeneity to subduction zone magmatism and the origin of EM1. Earth Planet Sci Lett 472:216–228
- Walker BA, Bergantz GW, Otamendi JE, Ducea MN, Cristofolini EA (2015) A MASH zone revealed: the mafic complex of the Sierra



69 Page 24 of 24 Bull Volcanol (2020) 82:69

Valle Fértil. J Petrol 56:1863–1896. https://doi.org/10.1093/petrology/egv057

- Wallace PJ, Carmichael IS (1999) Quaternary volcanism near the Valley of Mexico: implications for subduction zone magmatism and the effects of crustal thickness variations on primitive magma compositions. Contrib Mineral Petrol 135:291–314
- Wehrmann H, Hoernle K, Garbe-Schönberg D, Jacques G, Mahlke J, Schumann K (2014a) Insights from trace element geochemistry as
- to the roles of subduction zone geometry and subduction input on the chemistry of arc magmas. Int J Earth Sci 103:1929–1944
- Wehrmann H, Hoernle K, Jacques G, Garbe-Schönberg D, Schumann K, Mahlke J, Lara LE (2014b) Volatile (sulphur and chlorine), major, and trace element geochemistry of mafic to intermediate tephras from the Chilean Southern Volcanic Zone (33–43 S). Int J Earth Sci 103(7):1945–1962. https://doi.org/10.1007/S00531-014-1006-9

